

Borafluorenes | *Very Important Paper* |

VIP Highly Stable, Readily Reducible, Fluorescent, Trifluoromethylated 9-Borafluorenes

 Florian Rauch⁺, Sonja Fuchs⁺, Alexandra Friedrich, Daniel Sieh, Ivo Krummenacher, Holger Braunschweig, Maik Finze, and Todd B. Marder^{*[a]}

Abstract: Three different perfluoroalkylated borafluorenes (^FBf) were prepared and their electronic and photophysical properties were investigated. The systems have four trifluoromethyl moieties on the borafluorene moiety as well as two trifluoromethyl groups at the *ortho* positions of their *exo*-aryl moieties. They differ with regard to the *para* substituents on their *exo*-aryl moieties, being a proton (^FXyl^FBf, ^FXyl: 2,6-bis(trifluoromethyl)phenyl), a trifluoromethyl group (^FMes^FBf, ^FMes: 2,4,6-tris(trifluoromethyl)phenyl) or a dimethylamino group (*p*-NMe₂-^FXyl^FBf, *p*-NMe₂-^FXyl: 4-(dimethylamino)-2,6-bis(trifluoromethyl)phenyl), respectively. All derivatives exhibit extraordinarily low reduction potentials, compa-

rable to those of perylene diimides. The most electron-deficient derivative ^FMes^FBf was also chemically reduced and its radical anion isolated and characterized. Furthermore, all compounds exhibit very long fluorescent lifetimes of about 250 ns up to 1.6 μs; however, the underlying mechanisms responsible for this differ. The donor-substituted derivative *p*-NMe₂-^FXyl^FBf exhibits thermally activated delayed fluorescence (TADF) from a charge-transfer (CT) state, whereas the ^FMes^FBf and ^FXyl^FBf borafluorenes exhibit only weakly allowed locally excited (LE) transitions due to their symmetry and low transition-dipole moments.

Introduction

Boron-containing organic π -systems, especially triarylboranes^[1–13] and, more recently, boron-containing polyaromatics are of much current interest.^[3,10,14–20] Three-coordinate boron is isoelectronic with a carbonium ion, having an unoccupied p-orbital, making it inherently electron deficient and Lewis acidic. Thus, three-coordinate boranes can be employed as π -acceptors, single-electron or electron-pair acceptors. Such boranes have been used in linear^[21–40] and non-linear^[41–53] optical materials, anion sensors,^[8,54–56] frustrated Lewis pairs (FLPs),^[57–63] as well as in organic light-emitting diodes (OLEDs).^[64–66] There are numerous examples, both aromatic and antiaromatic, of boron-containing conjugated cyclic π -systems.^[16,20] The subclass of boroles is of special interest.^[3,18,67–82] They are isoelectronic with the antiaromatic cyclopentadiene

cation, having 4π electrons; however, the introduction of the boron vertex lowers the symmetry (Figure 1). This leads to a singlet ground state with a small HOMO–LUMO gap, resulting in the intense color of boroles, even though the molar extinction coefficient (ϵ) is quite small for their $S_1 \leftarrow S_0$ transitions.

Because of that, they are highly reactive towards nucleophiles and thereby unsuitable for many applications. Steric shielding, which works well for triarylboranes,^[33,83,84] only stabilizes boroles to a certain degree.^[79,85] Through benzannulation, the stability of boroles can be greatly increased,^[86–89] but the anti-aromatic character is significantly decreased due to delocalization of π -electron density over the biphenylene backbone. This leads to a stabilization of the HOMO as well as a destabilization of the LUMO resulting in a larger HOMO–LUMO gap and loss of the characteristic strong color of boroles. This also results in a lower Lewis acidity and, subsequently, significantly more stable systems.^[16,77] Detailed studies by Martin and co-workers demonstrate, however, that sterically less hindered derivatives, in particular, retain characteristic borole reactivity.^[90–94] Compared with their triarylborane derivatives, borafluorenes are usually more Lewis acidic and exhibit more positive reduction potentials.^[95] The stability of these systems can be further improved by sterically shielding^[87,88] or electronically saturating the boron center,^[86] through direct n-to-p conjugation or indirect F–B interaction (Figure 2).

Yamaguchi and co-workers reported air and moisture-stable borafluorene derivatives employing either Tip (2,4,6-tris(triisopropyl)phenyl) or the even bulkier Mes* (2,4,6-tris(*tert*-butyl)phenyl) substituents.^[86,87] It was found that the Tip derivatives could be used as turn-on type fluoride sensors, whereas the

[a] F. Rauch,⁺ S. Fuchs,⁺ Dr. A. Friedrich, Dr. D. Sieh, Dr. I. Krummenacher, Prof. Dr. H. Braunschweig, Prof. Dr. M. Finze, Prof. Dr. T. B. Marder
 Institute for Inorganic Chemistry and
 Institute for Sustainable Chemistry & Catalysis with Boron (ICB)
 Julius-Maximilians-Universität Würzburg
 Am Hubland, 97074 Würzburg (Germany)
 E-mail: todd.marder@uni-wuerzburg.de

[*] These authors have contributed equally to this work.

Supporting information and the ORCID identification number(s) for the author(s) of this article can be found under:
<https://doi.org/10.1002/chem.201905559>.

© 2020 The Authors. Published by Wiley-VCH GmbH. This is an open access article under the terms of the Creative Commons Attribution License, which permits use, distribution and reproduction in any medium, provided the original work is properly cited.

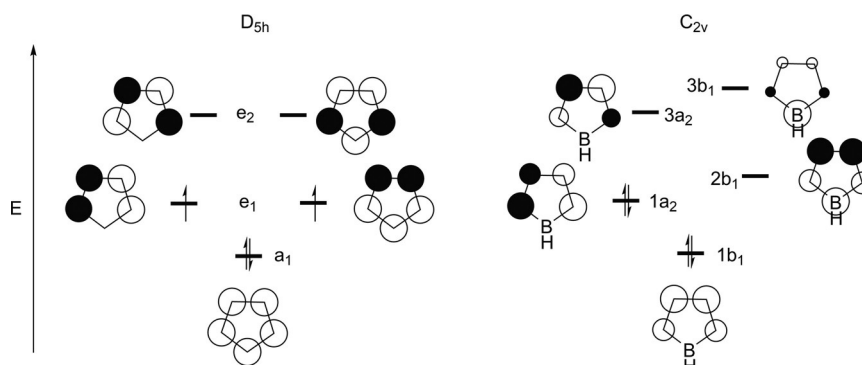


Figure 1. Frontier orbitals of the cyclopentadienyl cation (left) and borole (right).

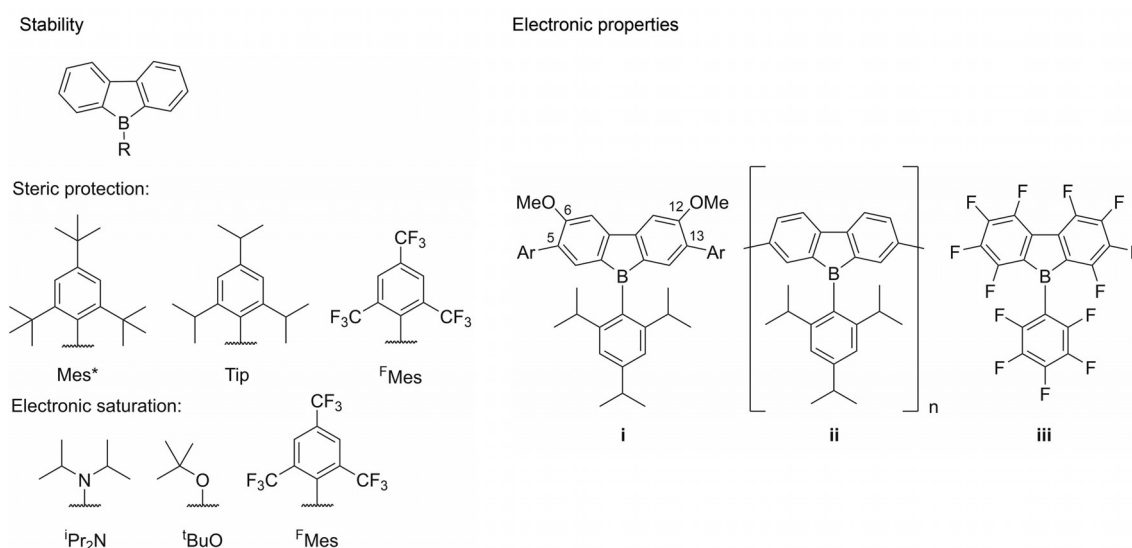


Figure 2. Selected examples of borafluorenes. A variety of *exo*-aryl substituents and the nature of their respective influence on the stability of the borafluorene (left).^[87,88] It is important to note, that *ortho*-trifluoromethyl substituted aryls provide both steric as well as electronic stabilization. Examples of the functionalization of the borafluorene backbone to tune the electronic properties (right).^[86,95–97]

Mes* compounds showed no reaction with fluoride. Recently, Rupar and co-workers have studied these effects in detail.^[88] They found that although Tip-substituted derivatives still decompose slowly (<10% decomp. over 24 h) in wet solvents, the corresponding ^FMes derivatives exhibit higher stability (5% decomp. over 24 h). Derivatives containing π -bonding moieties were found to be much more sensitive towards moisture (*i*PrN₂: 50% decomp. over 1 h; *t*BuO: 10% decomp. over 1 h). *ortho*-Trifluoromethyl-substituted aryls exhibit a strong stabilizing effect on boranes.^[33,79,98–102] In addition to the steric effect, a direct interaction of the lone pairs of the fluorine atoms with the empty p orbital of the boron center is observed. This is supported by B–F distances which are much shorter than the sum of their van der Waals radii (3.39 Å)^[103] in crystal structures. The electronic properties of borafluorenes can be easily tuned to fit different applications by the introduction of different substitution patterns on the biphenyl backbone (Figure 2, right). The introduction of methoxy groups at the 6 and 12 positions leads to a small hypsochromic shift of both the absorp-

tion and emission wavelength,^[86] whereas elongation of the π -system with electron-rich conjugated systems attached at the 5 and 13 positions leads to a bathochromic shift of both the absorption and emission wavelength.^[87] The photophysical properties of borafluorenes can also be modified by coordination of Lewis bases. Both Yamaguchi and co-workers and Rivard and co-workers observed turn-on fluorescence upon adduct formation.^[86,104] Wilson and Gillard and co-workers observed turn-off fluorescence of a borafluorene cation upon coordination of a Lewis base at low temperature, resulting in thermochromism.^[105] Piers and co-workers investigated the properties of a highly electron-deficient perfluorinated borafluorene **iii**.^[95,96] Although they only observed a reduction corresponding to the perfluoroaryls in the cyclic voltammogram, a reaction with the relatively mild reducing agent CoCp₂ (CoCp₂/CoCp₂⁺: –1.3 vs. Fc/Fc⁺) was observed, underlining the electron-deficient nature of the compound. In competition experiments with the strong Lewis acid B(C₆F₅)₃, preference towards the borafluorene derivative was observed, especially

with sterically demanding Lewis bases. The (sp²-C)–F bonds in this compound, however, are still reactive towards nucleophiles. In contrast, perfluoroalkyl groups are inert towards nucleophiles, provide a strong inductive electron-withdrawing effect and have been previously employed in the synthesis of electron-deficient triarylboranes.^[102] To the best of our knowledge, there have been no photophysical studies of borafluorenes with electron-deficient biphenyl backbones. We envisioned that judicious incorporation of trifluoromethyl groups both in the biphenyl core and at the *exo*-aryl moiety would provide a significant stability enhancement while retaining the low-lying LUMO typical of non-annulated boroles.

Results and Discussion

Synthesis

In order to maximize the stability of the trifluoromethylated borafluorenes (^FBf) we chose three different *meta*-fluoroxylene (1,3-bis(trifluoromethyl)benzene) derivatives as the *exo*-aryl moieties. To examine the influence of the *exo*-aryl and, specifically, substituents at the *para* position, we chose 2,6-bis(trifluoromethyl)phenyl (^FXyl), 2,4,6-tris(trifluoromethyl)phenyl (^FMes) and 4-(dimethylamino)-2,6-bis(trifluoromethyl)phenyl (*p*-NMe₂-^FXyl) groups (Scheme 1).

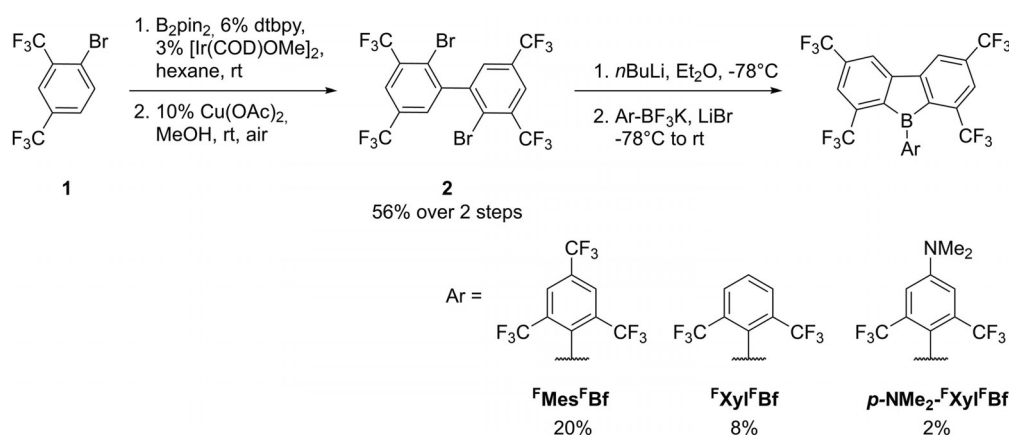
Biphenyl derivative **2** was synthesized through regioselective C–H borylation of **1**^[106,107] *ortho* to the bromine and a subsequent copper-catalyzed oxidative homocoupling. For the last step, **2** was dilithiated and subsequently reacted with the appropriate Ar-BF₃K salt. Attempts to synthesize the haloborafluorene with different BX₃ (X = F, Cl, Br) sources failed. Attempts to use aryl boronates in place of the Ar-BF₃K salt were also unsuccessful. The use of aryltrifluoroborate salts as boron source was previously reported by our group for the synthesis of boroles with enhanced stability,^[79] and applied by others in the synthesis of boron polyaromatic hydrocarbons (PAHs)^[108,109] and aryl borates.^[110,111] Organic trifluoroborate salts are widely employed in cross-coupling reactions as they are readily accessible and very stable.^[112,113] During the synthesis we observed that adding LiBr greatly improves the reactivity of the Ar-BF₃K

salts. It is possible that a cation-exchange reaction generates the more reactive Ar-BF₃Li salt. The increased reactivity of the Ar-BF₃Li salt is due to the thermodynamically favorable LiF elimination. It is also possible that LiBr stabilizes the aryllithium species towards decomposition in ethereal solvents. This decomposition also explains the low yields of isolated material. It is important to note that the corresponding *ortho*-trifluoromethylarylboron halides (X = Cl, Br) are not stable due to halide exchange.^[114] This might also explain why the synthesis of the haloborafluorenes was not possible. The compounds ^FMes^FBf, ^FXyl^FBf, and *p*-NMe₂-^FXyl^FBf were obtained after purification through sublimation and recrystallization. Both ^FMes^FBf and ^FXyl^FBf are bright-green solids. In contrast, *p*-NMe₂-^FXyl^FBf is a red solid. All compounds exhibit ¹H NMR and ¹³C{¹H} NMR signals consistent with their proposed structures. The ¹¹B{¹H} NMR shifts for all three borafluorene derivatives are around 64 ppm and differ only slightly. The ¹⁹F{¹H} NMR spectra display singlets and septets, the latter with a *J*_{FF} coupling constant of 3–4 Hz. (Table 1)

The singlets at about $\delta = -63.5$ ppm correspond to the two freely rotating *para* CF₃ groups on the borafluorene core. For ^FMes^FBf, another singlet corresponding to the *para* CF₃ group on the *exo*-aryl is observed. The CF₃ groups *ortho* to the boron center display a complex coupling pattern of two septets with small coupling constants (*J*_{FF} = 4 Hz). This can be attributed to through-space F–F coupling as previously observed at low temperature (243 K) for (^FMes)₂BAR compounds.^[100] The fact that the borafluorenes exhibit this phenomenon at room temperature is an indicator of the high rigidity of the systems.

Table 1. ¹¹B{¹H} and ¹⁹F{¹H} NMR shifts of ^FMes^FBf, ^FXyl^FBf, and *p*-NMe₂-^FXyl^FBf recorded in C₆D₆.

	^F Xyl ^F Bf	^F Mes ^F Bf	<i>p</i> -NMe ₂ - ^F Xyl ^F Bf
¹¹ B{ ¹ H} NMR [ppm]	63.2	64.1	64.7
¹⁹ F{ ¹ H} NMR [ppm]	–63.4	–62.0; –63.5	–63.4
singlet			
¹⁹ F{ ¹ H} NMR [ppm]	–58.2 (<i>J</i> _{FF} = 4 Hz)	–58.4 (<i>J</i> _{FF} = 4 Hz)	–58.1 (<i>J</i> _{FF} = 4 Hz)
septets	–59.6 (<i>J</i> _{FF} = 4 Hz)	–59.6 (<i>J</i> _{FF} = 4 Hz)	–59.5 (<i>J</i> _{FF} = 4 Hz)



Scheme 1. Synthesis of ^FMes^FBf, ^FXyl^FBf and *p*-NMe₂-^FXyl^FBf.

All three compounds are stable in the solid state and can be stored under ambient conditions without decomposition. In wet CDCl_3 (1.5 equiv. H_2O per borafluorene) at room temperature, no decomposition of either $^{\text{F}}\text{Mes}^{\text{F}}\text{Bf}$ or $^{\text{F}}\text{Xyl}^{\text{F}}\text{Bf}$ was observed over 4 days by NMR spectroscopy. This is surprising given that for $^{\text{F}}\text{MesBf}$ and TipBf , both less electron-deficient compounds, decomposition rates of 5 and 10% respectively in wet solvents over 24 h were reported.^[88] This indicates that the CF_3 -groups *ortho* to the boron center on the borafluorene core have a stabilizing effect, likely due to steric shielding. However, $p\text{-NMe}_2\text{-}^{\text{F}}\text{Xyl}^{\text{F}}\text{Bf}$ shows very rapid decomposition when exposed to wet solvents. It is likely that the dimethylamine moiety is protonated first, thereby further increasing the electrophilicity of the boron center and decreasing its stability towards nucleophilic attack. The reaction with H_2O leads to cleavage of one B–C bond of the borafluorene core, resulting in a BOH and CH moiety. The same reactivity towards water and other E–H bonds (E = N, O, S) was previously observed by Martin and co-workers.^[94] Likely due to less steric hindrance in their system, a second borafluorene reacts with the decomposition product to form a B–O–B motif. The product of the hydrolysis of $p\text{-NMe}_2\text{-}^{\text{F}}\text{Xyl}^{\text{F}}\text{Bf}$ was isolated and studied by X-ray diffraction (compound **D** in Figure S41, Supporting Information). All three compounds are slightly soluble in non-polar solvents such as hexane or toluene and soluble in polar non-coordinating solvents such as CH_2Cl_2 and THF. Dissolving $^{\text{F}}\text{Mes}^{\text{F}}\text{Bf}$ in acetonitrile gives a colorless solution. Investigation of the solution using ^{19}F NMR spectroscopy revealed the formation of an acetonitrile adduct, which is consistent with previous studies by Martin and co-workers for less sterically hindered borafluorenes.^[91] The *para*- CF_3 groups, both on the borafluorene backbone as well as the *exo*-aryl moiety, are influenced only weakly by the coordination of acetonitrile, because both singlets in the ^{19}F NMR spectrum shift only slightly to lower field.

The signals corresponding to the *ortho* CF_3 -groups, however, change dramatically. Instead of two septets as observed for $^{\text{F}}\text{Mes}^{\text{F}}\text{Bf}$, one septet at -51.9 ppm ($J_{\text{FF}} = 10$ Hz), one broad singlet at -56.2 , and a quartet at -60.7 ppm ($J_{\text{FF}} = 10$ Hz), are observed (Figure 3, middle).

This suggests that only one *exo*-aryl trifluoromethyl moiety is coupling to the *ortho* trifluoromethyl groups on the borafluorene backbone. After evaporation of the acetonitrile and dissolution in C_6D_6 , only the borafluorene was observed through ^{19}F NMR spectroscopy. Thus, the formation of the adduct with acetonitrile is completely reversible.

Crystal and molecular structures

Single crystals of the three borafluorenes as well as the acetonitrile adduct of $^{\text{F}}\text{Mes}^{\text{F}}\text{Bf}$ ($^{\text{F}}\text{Mes}^{\text{F}}\text{Bf}\cdot\text{MeCN}$) suitable for X-ray studies were obtained (Figure 4) and selected bond lengths, angles, torsion angles and short B–F contacts are listed in Table 2. The single crystals of $^{\text{F}}\text{Mes}^{\text{F}}\text{Bf}$ and $p\text{-NMe}_2\text{-}^{\text{F}}\text{Xyl}^{\text{F}}\text{Bf}$ were obtained from a saturated hexane solution at -30°C , that of $^{\text{F}}\text{Xyl}^{\text{F}}\text{Bf}$ was obtained by evaporation of a saturated CH_2Cl_2 solution and that of $^{\text{F}}\text{Mes}^{\text{F}}\text{Bf}\cdot\text{MeCN}$ was obtained from a saturated acetonitrile solution at -30°C .

A comparison of the crystal structures of the three target compounds shows the following. Although all three B–C bond lengths are in a similar range for $^{\text{F}}\text{Mes}^{\text{F}}\text{Bf}$ (1.579(3)–1.591(3) Å), the B–C_{1_{exo}} distances to the $^{\text{F}}\text{Xyl}$ groups of $^{\text{F}}\text{Xyl}^{\text{F}}\text{Bf}$ and $p\text{-NMe}_2\text{-}^{\text{F}}\text{Xyl}^{\text{F}}\text{Bf}$ (B–C = 1.570(3) Å) are slightly shorter than the respective B–C2 and B–C3 bonds (1.591(3)–1.595(3) Å) within the borole moieties (Table 2). The boron atoms have a nearly ideal trigonal-planar configuration with the sum of the C–B–C angles being $359.74(16)$ – $359.99(16)^\circ$. In all three compounds, the C2–B–C3 angle ($102.94(14)$ – $103.95(15)^\circ$) within the borole moiety is much smaller than the other two C–B–C angles. The borole

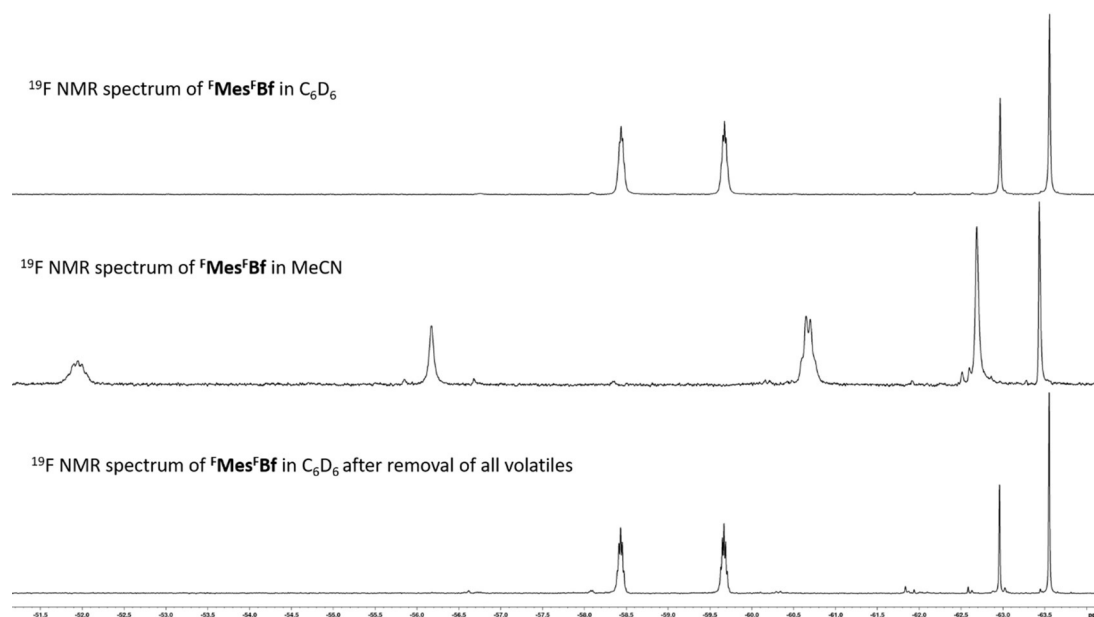


Figure 3. ^{19}F NMR spectra (188 MHz, 298 K) of $^{\text{F}}\text{Mes}^{\text{F}}\text{Bf}$ in C_6D_6 (top), in CH_3CN (middle) and in C_6D_6 after removal of all volatiles (bottom).

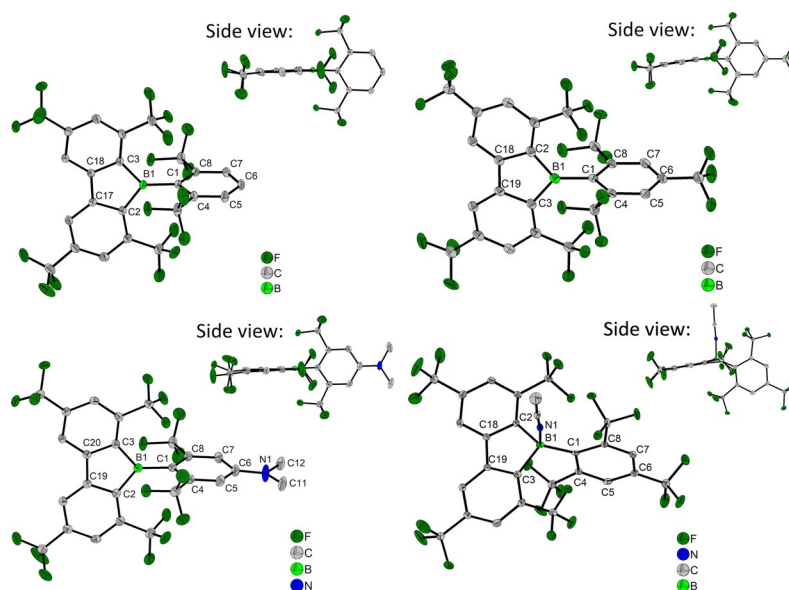


Figure 4. Molecular structures of $^{\text{F}}\text{Xyl}^{\text{F}}\text{Bf}$ (top left), $^{\text{F}}\text{Mes}^{\text{F}}\text{Bf}$ (top right), $p\text{-NMe}_2\text{-}^{\text{F}}\text{Xyl}^{\text{F}}\text{Bf}$ (bottom left) and $^{\text{F}}\text{Mes}^{\text{F}}\text{Bf-MeCN}$ (bottom right) determined by single-crystal X-ray diffraction at 100 K. All ellipsoids are drawn at the 50% probability level, and H atoms and solvent molecules are omitted for clarity.

Table 2. Selected bond lengths [Å] and angles [°] in $^{\text{F}}\text{Mes}^{\text{F}}\text{Bf}$, $^{\text{F}}\text{Xyl}^{\text{F}}\text{Bf}$, $p\text{-NMe}_2\text{-}^{\text{F}}\text{Xyl}^{\text{F}}\text{Bf}$ and $^{\text{F}}\text{Mes}^{\text{F}}\text{Bf-MeCN}$. Atom labels for the respective molecular structures are shown in Figure 4.

	$^{\text{F}}\text{Mes}^{\text{F}}\text{Bf}$	$^{\text{F}}\text{Xyl}^{\text{F}}\text{Bf}$	$p\text{-NMe}_2\text{-}^{\text{F}}\text{Xyl}^{\text{F}}\text{Bf}$	$^{\text{F}}\text{Mes}^{\text{F}}\text{Bf-MeCN}$
B–C1	1.579(3)	1.570(2)	1.570(3)	1.652(3)
B–C2	1.581(3)	1.591(3)	1.595(3)	1.645(3)
B–C3	1.591(3)	1.591(3)	1.591(3)	1.645(3)
B–N				1.591(3)
C3–C19/C18/C20	1.408(3)	1.410(2)	1.409(2)	1.401(3)
C2–C18/C17/C19	1.410(2)	1.409(2)	1.408(2)	1.410(3)
C18/C17/C19–C19/C18/C20	1.481(3)	1.474(2)	1.482(2)	1.475(3)
\sphericalangle BC ₃ –Aryl _{exo}	89.32(7)	89.84(8)	89.27(6)	
\sphericalangle BC ₁₂ –Aryl _{exo}	89.43(6)	89.54(6)	88.69(5)	82.12(6)
torsion of Ar _{exo} out of borafluorene plane	171.28(16)	176.45(16)	178.83(17)	137.6(2)
\sphericalangle C1–B–C2–C18/C17/C19				
5-ring: \sphericalangle C2BC3	103.95(15)	103.07(13)	102.94(14)	99.74(18)
Sum \sphericalangle CBC	359.74(16)	359.90(15)	359.99(16)	338.43(18)
sum \sphericalangle CNC			359.84(19)	
shortest B–F contact(s)	2.392(3) 2.440(3)	2.379(2) 2.390(3)	2.366(2) 2.434(2)	2.853(3)

moiety shows similar bond lengths and angles in all three compounds. The angles increase from C–B–C to B–C–C (106.57(16)–107.52(15)°) and to C–C–C (110.98(17)–111.41(15)°). The C2–C and C3–C bond lengths (1.408(3)–1.410(2) Å) are typical for aromatic bonds, whereas the C–C bond (1.474(2)–1.482(2) Å) that is opposite to the boron atom has significant single-bond character. The interplanar angle between the borafluorene (BC₁₂) and the *exo*-aryl substituent is close to 90° in all three compounds (88.69(5)–89.54(6)°). This is due to the large steric demand of the CF₃ groups in the *ortho* positions of both the *exo*-aryl moiety as well as the borafluorene core. In all three compounds, two B–F distances, each in the range of 2.366(2)–2.440(3) Å, are observed, which are significantly shorter than the sum of the van der Waals radii for boron and fluorine (3.39 Å).^[103] This was previously observed in boranes and boroles with *ortho*-CF₃ aryl moieties.^[33,79,102,114,115] Given that

the two respective fluorine atoms are directly above and below the boron center, it is most likely that the lone pair electrons of these fluorine atoms interact with the empty p-orbital of the boron center. The torsion angle C_{endo}-C2_{endo}-B-C1_{exo} with the *endo* carbon atoms belonging to the borole moiety deviates slightly from 180° (171.28(16)–178.83(17)°). This shows that the B–C1 bond to the exocyclic moiety is tilted slightly out of the borafluorene plane. The out-of-plane tilt increases from $p\text{-NMe}_2\text{-}^{\text{F}}\text{Xyl}^{\text{F}}\text{Bf}$ (1.17(17)°) to $^{\text{F}}\text{Xyl}^{\text{F}}\text{Bf}$ (3.55(16)°) and $^{\text{F}}\text{Mes}^{\text{F}}\text{Bf}$ (8.72(16)°). The magnitude of the tilt is related to the molecular packing, which is similar in all three crystal structures because the borafluorene moieties are arranged in pairs, which are related by inversion symmetry and form weak intermolecular $\pi\cdots\pi$ interactions between the borafluorene backbones. The strongest $\pi\cdots\pi$ interaction is observed in $^{\text{F}}\text{Mes}^{\text{F}}\text{Bf}$, which shows the smallest centroid– distance, interplanar sepa-

ration, and offset shift (Table S3, Supporting Information). Hence, these pairs of molecules are closest in ${}^{\text{F}}\text{Mes}^{\text{F}}\text{Bf}$, and the exocyclic ${}^{\text{F}}\text{Mes}$ moiety is tilted out of the plane the most, away from the center of the pair in order to avoid close F...F contacts between the two molecules. In the crystal structure of the acetonitrile adduct of ${}^{\text{F}}\text{Mes}^{\text{F}}\text{Bf}$, as the hybridization at the boron is now sp^3 rather than sp^2 , all of the B–C bonds are elongated. The C2–B1–C3 angle of the borole ring ($99.74(18)^\circ$) is decreased compared to ${}^{\text{F}}\text{Mes}^{\text{F}}\text{Bf}$ ($103.95(15)^\circ$). The torsion angle of the *exo*-aryl towards the borafluorene backbone is decreased ($82.12(6)^\circ$) and the bending of the *exo*-aryl out of the plane of the borafluorene moiety ($137.6(2)^\circ$) deviates significantly from 180° . In the adduct, there is only one short B–F contact ($\text{F3}–\text{B1}=2.853(3) \text{ \AA}$) that is elongated compared to ${}^{\text{F}}\text{Mes}^{\text{F}}\text{Bf}$, but still shorter than the sum of the van der Waals radii. The B–N bond length is $1.591(3) \text{ \AA}$, which is significantly shorter than that in the acetonitrile adduct of $\text{B}(\text{C}_6\text{F}_6)_3$ ($1.616(3) \text{ \AA}$),^[116] but similar to that in the previously reported MeCN adduct of PhBf ($\text{PhBf}\cdot\text{MeCN}$) ($1.598(4) \text{ \AA}$).^[91] The $\text{N}\equiv\text{C}$ bond ($1.129(3) \text{ \AA}$) is also shorter than that in the acetonitrile adduct of $\text{B}(\text{C}_6\text{F}_6)_3$ ($1.141(2) \text{ \AA}$) and very similar to that in $\text{PhBf}\cdot\text{MeCN}$ ($1.128(4) \text{ \AA}$).

Electrochemistry

Cyclic voltammograms of the three borafluorenes were recorded in dichloromethane with $[n\text{Bu}_4\text{N}][\text{PF}_6]$ as the electrolyte and a scan rate of 250 mV s^{-1} (Figure 5) in order to determine their reduction potentials. All measurements were referenced to the ferrocene/ferrocenium redox couple (Fc/Fc^+). The most electron-deficient borafluorene, ${}^{\text{F}}\text{Mes}^{\text{F}}\text{Bf}$, exhibits a reversible reduction at -1.13 V and an irreversible reduction at -2.04 V . For the slightly less electron-deficient ${}^{\text{F}}\text{Xyl}^{\text{F}}\text{Bf}$, a reversible reduction at -1.21 V and an irreversible reduction at -2.12 V are observed. Interestingly, *p*- NMe_2 - ${}^{\text{F}}\text{Xyl}^{\text{F}}\text{Bf}$ shows a reversible reduction at -1.28 V , an irreversible reduction at -2.15 V and a partially reversible oxidation at 0.95 V .

The three borafluorenes exhibit much higher reduction potentials (${}^{\text{F}}\text{Mes}^{\text{F}}\text{Bf}=-1.13 \text{ V}$; ${}^{\text{F}}\text{Xyl}^{\text{F}}\text{Bf}=-1.21 \text{ V}$ and *p*- NMe_2 - ${}^{\text{F}}\text{Xyl}^{\text{F}}\text{Bf}=-1.28 \text{ V}$) than any of the previously reported borafluorenes and boroles or triarylboranes (Table 3). The substitution patterns of compounds ${}^{\text{F}}\text{MesBC}_4\text{Ph}_4$ ($E_{1/2}=-1.52 \text{ V}$) and ${}^{\text{F}}\text{MesBf}$ ($E_{1/2}=-1.82 \text{ eV}$) allows a direct comparison of the fluorinated borafluorene backbone (${}^{\text{F}}\text{Bf}$) with the unsubstituted borafluorene backbone (Bf) and the non-annulated borole.^[88] The strong anodic shift of the ${}^{\text{F}}\text{Mes}^{\text{F}}\text{Bf}$ as compared to ${}^{\text{F}}\text{MesBC}_4\text{Ph}_4$ and ${}^{\text{F}}\text{MesBf}$ demonstrates the strong electron-withdrawing effect of the CF_3 groups on the borafluorene

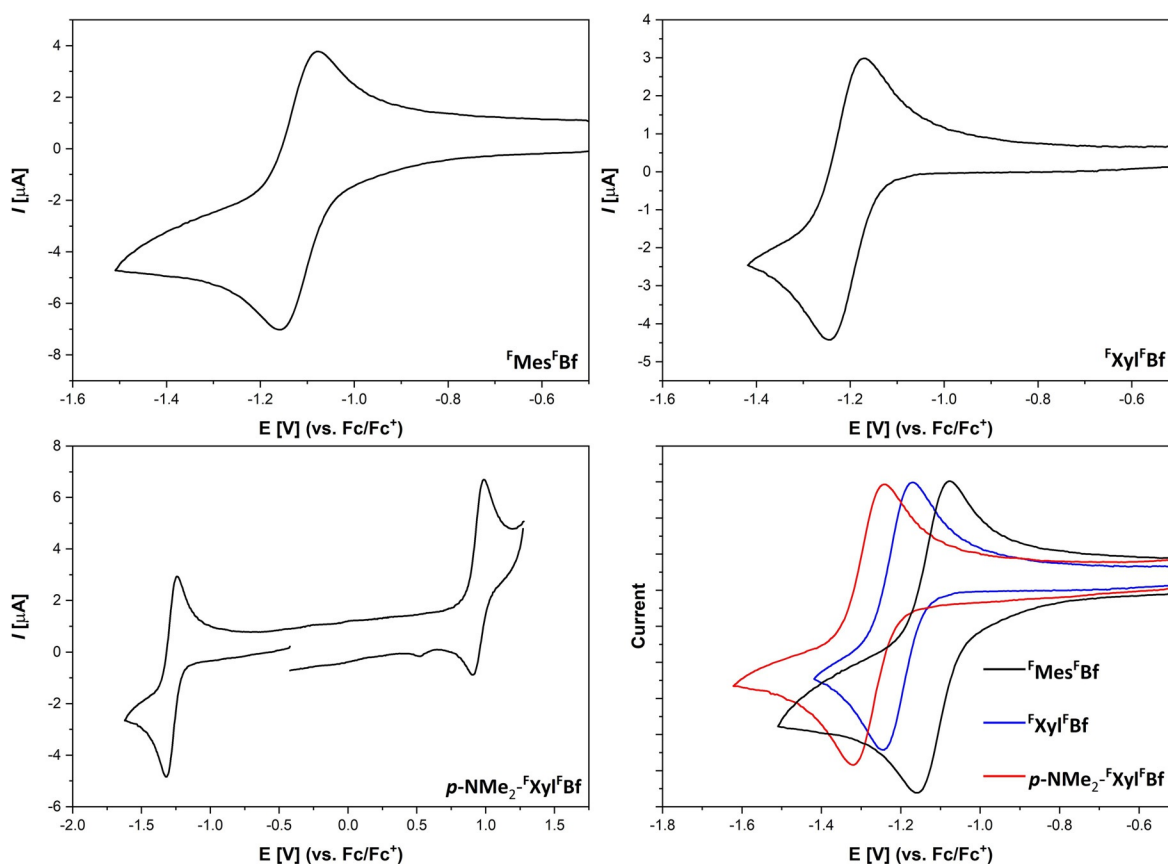
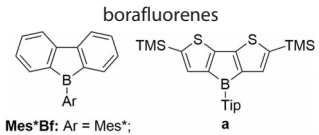
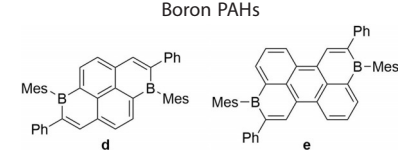
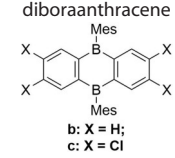


Figure 5. Cyclic voltammograms of the reversible redox events of ${}^{\text{F}}\text{Mes}^{\text{F}}\text{Bf}$ (top left), ${}^{\text{F}}\text{Xyl}^{\text{F}}\text{Bf}$ (top right) and *p*- NMe_2 - ${}^{\text{F}}\text{Xyl}^{\text{F}}\text{Bf}$ (bottom left). All samples are referenced against the Fc/Fc^+ redox couple. For better comparison, the reduction waves are plotted together (bottom right; ${}^{\text{F}}\text{Mes}^{\text{F}}\text{Bf}$ (black), ${}^{\text{F}}\text{Xyl}^{\text{F}}\text{Bf}$ (blue), *p*- NMe_2 - ${}^{\text{F}}\text{Xyl}^{\text{F}}\text{Bf}$ (red)).

Table 3. Tabulated first reduction potential values of various three-coordinate boron species.

Compound	First reduction potential $E_{1/2}$ [V] vs. Fc/Fc ⁺ this work	Compound	First reduction potential $E_{1/2}$ [V] vs. Fc/Fc ⁺
FMesFBfa	−1.13	free boroles	
FMesFBfa	−1.21	PhBC₄Ph₄ : Ar = Ph;	
p-NMe2-FXylFBfa	−1.28	MesBC₄Ph₄ : Ar = Mes;	
		^FMesBC₄Ph₄ : Ar = ^F Mes	
		PhBC₄Ph₄ ^a	−1.61 ^[117]
Mes[*]Bf^d : Ar = Mes [*] ;		MesBC₄Ph₄ ^a	−1.69 ^[85, 117, 118]
TipBf^e : Ar = Tip;		^FMesBC₄Ph₄ ^a	−1.52 ^[79]
^FMesBf^e : Ar = ^F Mes		Boron PAHs	
Mes[*]Bf^d	−2.28 ^[87]		
TipBf^e	−2.14 ^[88]	d^a	−1.15 ^[120]
^FMesBf^e	−1.82 ^[88]	e^a	−1.07 ^[120]
a^f	−1.98 ^[119]	triaryl boranes	
		B(3,5-(CF₃)₂C₆H₃)₃^c	−1.61 ^[102]
b^g : X = H;	−1.84 ^[15]	B(2,4-(CF₃)₂C₆H₃)₃^c	−1.79 ^[102]
c^g : X = Cl	−1.38 ^[31]	B(2,5-(CF₃)₂C₆H₃)₃^c	−1.85 ^[102]
B(Mes)₃^b	−2.73 ^[121]		
B(Mes)₂(C₆F₅)^b	−2.10 ^[121]		
B(Mes)(C₆F₅)₂^b	−1.72 ^[121]		
B(C₆F₅)₃^a	−1.97 ^[77]		

Measurement conditions: [a] Platinum electrode, CH₂Cl₂ (solvent), [nBu₄N][PF₆] (electrolyte); [b] Platinum electrode, THF (solvent), [nBu₄N][B(C₆F₅)₄] (electrolyte); [c] Glassy carbon electrode, CH₂Cl₂ (solvent), [nBu₄N][B(C₆F₅)₄] (electrolyte); [d] Glassy carbon electrode, THF (solvent), [nBu₄N][ClO₄] (electrolyte); [e] Glassy carbon electrode, CH₂Cl₂ (solvent), [nBu₄N][PF₆] (electrolyte); [f] Glassy carbon electrode, THF (solvent), [nBu₄N][PF₆] (electrolyte); [g] Platinum electrode, THF (solvent), [nBu₄N][PF₆] (electrolyte).

backbone. This is likely due to the planar geometry as well as the fact that the *ortho* CF₃-groups of the borafluorene backbone do not display B–F interactions, and thus do not increase electron density at the boron atom. The reduction potentials of the trifluoromethylated borafluorenes do not differ strongly from one another. This indicates that the *para* substituent on the *exo*-cyclic aryl moiety does not have a significant influence on the electron accepting properties of these borafluorenes. This is best illustrated by the fact that the π -donating dimethylamino group only leads to a cathodic shift of 0.15 V compared to a trifluoromethyl group. This is likely due to the nearly perpendicular arrangement of the *exo*-aryl group with respect to the borafluorene backbone, that limits π -conjugation leaving only inductive effects of the *exo*-aryl moiety on the borafluorene core and the boron center. To investigate further the electronic properties of borafluorene ^FMes^FBf, CoCp₂ was chosen as a reducing agent ($E^0(\text{CoCp}_2) = -1.3$ V vs. Fc/Fc⁺).^[122] Thus, after addition of CoCp₂, the yellowish THF solution of ^FMes^FBf turned dark purple and an ESR measurement confirmed the presence of the borafluorene radical anion [^FMes^FBf]^{•−} (Figure 6).

A THF solution of the radical anion [^FMes^FBf]^{•−} shows a complex EPR signal centered at $g_{\text{iso}} = 2.004$ consisting of hyperfine splittings to boron ($a(^{11}\text{B}) = 3.3$ G; see non-annulated borole

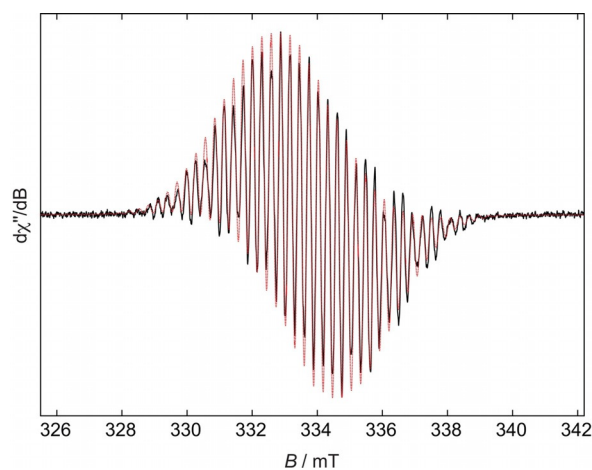


Figure 6. Experimental (black solid line) and simulated (red dashed line) continuous-wave X-band EPR spectra of [^FMes^FBf]^{•−} in a THF solution at room temperature.

derivatives ($a(^{11}\text{B}) = 3.4$ – 3.7 G)^[85, 123], the CF₃ fluorine atoms ($a(^{19}\text{F}) = 11.3$ and 6.0 G) and the hydrogen atoms ($a(^1\text{H}) = 6.1$ and 2.9 G) of the borafluorene core. The relatively small boron hyperfine coupling together with the relatively large proton and fluorine hyperfine couplings indicate significant spin de-

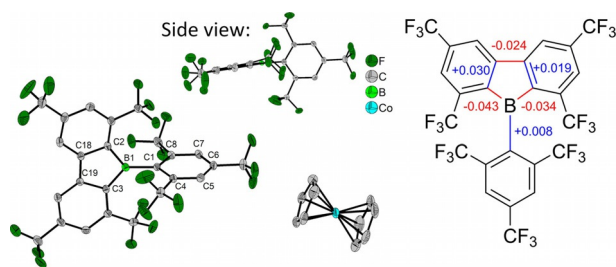


Figure 7. The solid-state molecular structure of $[\text{F}^{\text{Mes}}\text{Fbf}]^{\cdot -}$ determined by single-crystal X-ray diffraction at 100 K. All ellipsoids are drawn at the 50% probability level. H atoms and THF solvent molecules are omitted for clarity. Only half of the symmetrically non-equivalent molecules are shown. One of the CF_3 groups on the borafluorene core is rotationally disordered and only the part with the higher occupancy (64%) is shown here (left). The relevant changes in bond lengths of $[\text{F}^{\text{Mes}}\text{Fbf}]^{\cdot -}$ compared to the neutral starting material are shown at the right.

localization onto the benzene rings, to a greater extent than in other singly reduced borafluorenes.^[87]

Crystals of the radical anion suitable for X-ray diffraction were obtained by slow diffusion of pentane into a saturated THF solution (Figure 7). Upon reduction, a variety of changes in the structure are observed. As there are two independent molecules in the unit cell for the radical anion, both molecules are taken into account for comparison (Table S2, Supporting Information). The negative charge is apparently localized on the borafluorene core, as the *exo*-aryl moiety is only slightly influenced, with almost all changes in bond length being within

3 esd's. Although the B–C1 bond length is slightly increased ($\Delta(\text{B}-\text{C}1) = +0.008$ and $+0.015$ Å), both borafluorene B–C bonds (B–C2 and B–C3) are shortened ($\Delta(\text{B}-\text{C}2) = -0.034$ and -0.025 Å; $\Delta(\text{B}-\text{C}3) = -0.043$ and -0.040 Å). The neighboring borafluorene C–C bonds are elongated ($\Delta(\text{C}3-\text{C}19) = +0.030$ and $+0.027$ Å; $\Delta(\text{C}2-\text{C}18) = +0.019$ and $+0.022$ Å) and the C–C bond connecting the two borafluorene aryls is shortened ($\Delta(\text{C}18-\text{C}19) = -0.024$ Å). In summary, the bond lengths within the five-membered heterocycle equalize. This behavior was previously observed in the structures of borole radical anions and dianions.^[85] The one-electron reduction also influences the shortest B–F distances which are elongated (mean $\Delta(\text{B}-\text{F}) = +0.278$ Å).

Photophysical properties

To obtain further insight into the electronic structure of the borafluorenes, absorption and emission spectra as well as quantum yields and excited-state lifetimes were measured in hexane (Figure 8 and Table 4). Furthermore, $\text{F}^{\text{Mes}}\text{Fbf}$ was also studied in CH_2Cl_2 and in the solid state. Solvatochromic studies of $p\text{-NMe}_2\text{-F}^{\text{Xyl}}\text{Fbf}$ could not be carried out, because no emission was detected in more polar solvents. This is most likely due to a further redshift of the emission, which in turn results in increased non-radiative decay processes and thus a much lower quantum yield. A photophysical investigation of $\text{F}^{\text{Mes}}\text{Fbf}\text{-MeCN}$ is included in the Supporting Information (see also Figure S50 and Table S5).

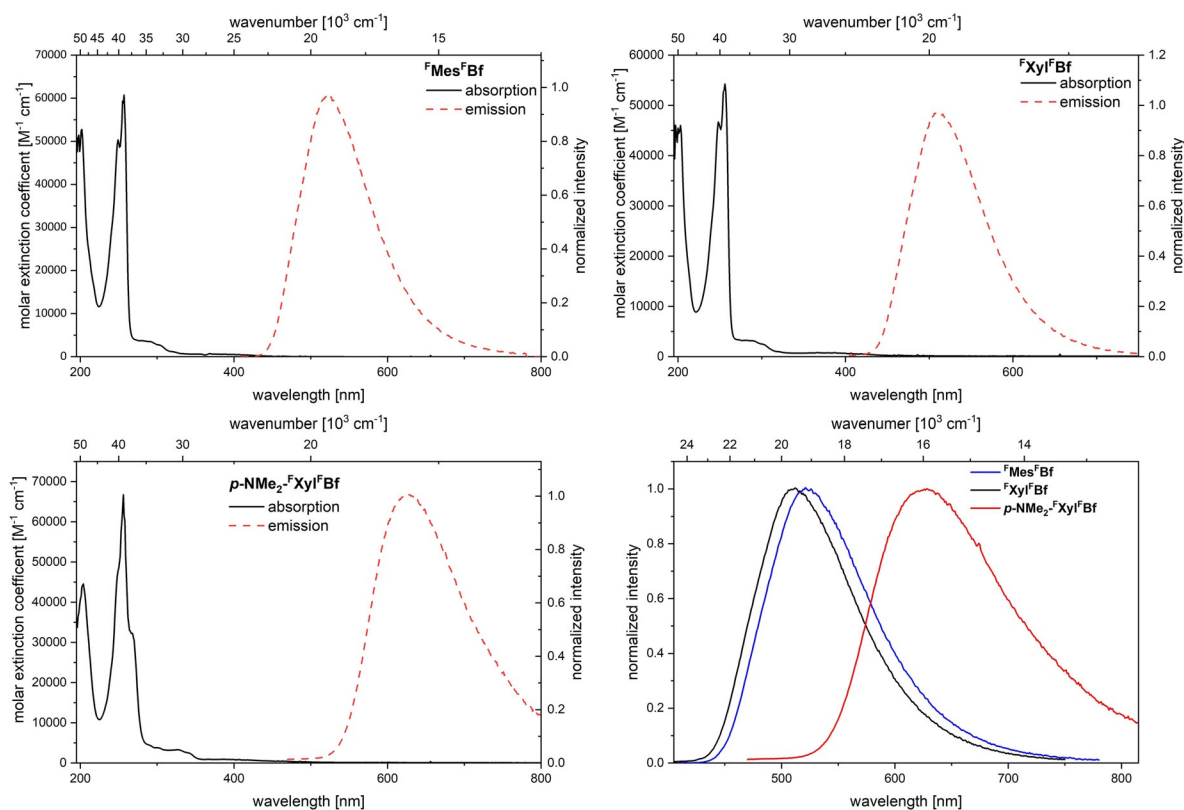


Figure 8. Absorption (black) and emission spectra (red) in hexane of $\text{F}^{\text{Mes}}\text{Fbf}$ (top left), $\text{F}^{\text{Xyl}}\text{Fbf}$ (top right) and $p\text{-NMe}_2\text{-F}^{\text{Xyl}}\text{Fbf}$ (bottom left). For comparison, the emission spectra are plotted together (bottom right; $\text{F}^{\text{Mes}}\text{Fbf}$ (black), $\text{F}^{\text{Xyl}}\text{Fbf}$ (blue), $p\text{-NMe}_2\text{-F}^{\text{Xyl}}\text{Fbf}$ (red)).

Table 4. Photophysical data for borafluorenes ^FMes^FBf, ^FXyl^FBf, and *p*-NMe₂-^FXyl^FBf.

Compound	Solvent	λ_{abs} [nm] (ϵ [10 ³ M ⁻¹ cm ⁻¹]; log ϵ)	λ_{em} [nm] ^[a]	Apparent Stokes shift [10 ³ cm ⁻¹]	Φ_{fl}	τ [ns] (rel %)	τ_0 [ns]	k_{nr} [10 ⁷ s ⁻¹] ^[b]	k_r [10 ⁷ s ⁻¹] ^[c]
^F Mes ^F Bf	hexane	290 (2.9; 3.46), 321 (0.8; 2.90), 400 (0.3; 2.48)	521	5.8	0.37	224	605	0.3	0.2
	CH ₂ Cl ₂	395	540	6.8	0.18	151	835	0.1	0.005
	solid	405	527	6.0	0.06	173	2557	0.5	0.04
^F Xyl ^F Bf	hexane	256 (54.2; 4.73), 290 (2.9; 3.46), 386 (0.4; 2.60)	510	6.3	0.30	249	820	0.3	0.1
<i>p</i> -NMe ₂ - ^F Xyl ^F Bf	hexane	268 (32.3; 4.51), 326 (2.7; 3.43), 396 (0.3; 2.48)	627	9.3	0.03	9.2 (64%), 1626 (36%)	–	–	–

[a] Excited at the respective $\lambda_{\text{abs, max}}$ of the $S_1 \leftarrow S_0$ transition. [b] The non-radiative rate constants were calculated from $k_{\text{nr}} = (1 - \Phi_{\text{fl}}) / \tau$. [c] The radiative rate constants were calculated from $k_r = \Phi_{\text{fl}} / \tau$.

All borafluorenes exhibit very small extinction coefficients for their lowest-energy absorption ($\epsilon = 300\text{--}400 \text{ M}^{-1} \text{ cm}^{-1}$; $\log \epsilon = 2.48\text{--}2.60$) which can be classified as weakly allowed transitions,^[124] similar to those in previously reported boroles and borafluorenes. The lowest-energy absorption of ^FXyl^FBf ($\lambda_{\text{abs, max}} = 386 \text{ nm}$) appears to be slightly hypsochromically shifted compared to ^FMes^FBf ($\lambda_{\text{abs, max}} = 400 \text{ nm}$) and *p*-NMe₂-^FXyl^FBf ($\lambda_{\text{abs, max}} = 396 \text{ nm}$) but, due to the broad absorption bands, this is difficult to determine accurately. All three borafluorenes exhibit broad, structureless emission bands. The emission maximum of *p*-NMe₂-^FXyl^FBf is strongly bathochromically shifted ($\lambda_{\text{em, max}} = 627 \text{ nm}$) compared to the two non-donor-substituted borafluorene derivatives (^FMes^FBf: $\lambda_{\text{em, max}} = 521 \text{ nm}$; ^FXyl^FBf: $\lambda_{\text{em, max}} = 510 \text{ nm}$), which indicates that the emission arises from an intramolecular charge-transfer (ICT) transition. The quantum yields of ^FMes^FBf ($\Phi_{\text{fl}} = 0.37$; hexane) and ^FXyl^FBf ($\Phi_{\text{fl}} = 0.30$; hexane) are higher than most of the reported borafluorenes (ca. 0.1). In contrast, *p*-NMe₂-^FXyl^FBf exhibits a very low quantum yield ($\Phi_{\text{fl}} = 0.03$; hexane). To our surprise, ^FMes^FBf and ^FXyl^FBf exhibit very long fluorescent lifetimes in solution (^FMes^FBf: $\tau = 224 \text{ ns}$ (hexane); $\tau = 151 \text{ ns}$ (CH₂Cl₂); ^FXyl^FBf: $\tau = 249 \text{ ns}$ (hexane)) as well as in the solid state (^FMes^FBf: $\tau = 173 \text{ ns}$). Similar fluorescence lifetimes (116–150 ns) of borafluorenes with bulky *exo*-aryl moieties were previously observed by Rupar and co-workers.^[89] This results in exceptionally long natural lifetimes, τ_0 , uncommon for organic molecules, for which fluorescence usually takes place on a nanosecond timescale. There are, however, some exceptions such as pyrene.^[36, 125, 126] This indicates a forbidden process. It is very interesting that even though the radiative rate constants are small for organic chromophores, the non-radiative rate constants are of the same order, resulting in moderate quantum yields. This is likely a result of the high rigidity of the systems. In contrast, *p*-NMe₂-^FXyl^FBf exhibits two different radiative decay processes, a prompt ($\tau = 9.2 \text{ ns}$) and a delayed ($\tau = 1.6 \mu\text{s}$) one. This can be caused by different processes namely TTA (triplet–triplet annihilation)^[127] or TADF (thermally activated delayed fluorescence).^[66, 128–142] Due to the low concentrations ($\leq 10^{-5} \text{ M}$) of the compound employed, the lack of dependence on the concentration and the temperature dependence of the

lifetime, we can attribute the observed behavior to TADF. The mechanism for TADF is based on a reverse intersystem crossing process (rISC) between the lowest-energy triplet state (T_1) and excited singlet state (S_1) of a molecule. In order for this to occur, the energy difference between S_1 and T_1 (ΔE_{S-T}) has to be sufficiently small. The most common structures to exhibit this phenomenon are twisted dipolar systems with spatially separated HOMO and LUMO such as D(donor)– π –A(acceptor) compounds. This structural motif is also found in *p*-NMe₂-^FXyl^FBf. The singlet–triplet gap (ΔE_{S-T}) can be easily determined experimentally if phosphorescence can be observed. However, for *p*-NMe₂-^FXyl^FBf, even at 77 K in a frozen glass matrix of 2-MeTHF, no phosphorescence was observed. However, ΔE_{S-T} can also be calculated once the rate constant of the rISC process (k_{rISC}) is obtained, which is given by the Arrhenius Equation (1), or Equation (2) as derived by Dias et al.^[143]

$$k_{\text{rISC}} = A \exp\left(-\frac{\Delta E_{S-T}}{kT}\right) \quad (1)$$

$$k_{\text{rISC}} = \frac{\Phi_{\text{rISC}}}{\tau_{\text{DF}}} \left(\frac{\Phi_{\text{PF}} + \Phi_{\text{DF}}}{\Phi_{\text{PF}}}\right) \quad (2)$$

with Φ_{DF} , Φ_{PF} and Φ_{rISC} being the quantum yields of the delayed and prompt fluorescence and the reverse intersystem crossing, respectively. Given that no phosphorescence was observed at 77 K, but delayed fluorescence was, it can be assumed that ΔE_{S-T} is small and, as such, the rate of reverse intersystem crossing is very high, i.e.,

$$\Phi_{\text{rISC}} = \frac{k_{\text{rISC}}}{k_{\text{rISC}} + k_{\text{IC}} + k_{\text{PH}}} \approx 1$$

and, thus, Equation (2) can be modified to give Equation (3).

$$k_{\text{rISC}} = \frac{1}{\tau_{\text{DF}}} \left(\frac{\Phi_{\text{PF}} + \Phi_{\text{DF}}}{\Phi_{\text{PF}}}\right) = \frac{1}{\tau_{\text{DF}}} \left(1 + \frac{\Phi_{\text{DF}}}{\Phi_{\text{PF}}}\right) = \frac{1}{\tau_{\text{DF}}} + \frac{1}{\tau_{\text{DF}}} * \frac{\Phi_{\text{DF}}}{\Phi_{\text{PF}}} \quad (3)$$

The ratio $\Phi_{\text{DF}}/\Phi_{\text{PF}}$ can be ascertained from time-resolved measurements via Equation (4),

$$\frac{\Phi_{\text{DF}}}{\Phi_{\text{PF}}} = \frac{B_{\text{DF}} \tau_{\text{DF}}}{B_{\text{PF}} \tau_{\text{DF}}} \quad (4)$$

with B_{DF} and B_{PF} being the pre-exponential fitting parameters of the time-resolved fluorescence lifetime measurements. As such, equation (1) can be written as Equation (5) where all parameters can be obtained from the time-resolved fluorescence decay.

$$k_{\text{risc}} = A \exp\left(-\frac{\Delta E_{S-T}}{kT}\right) = \frac{1}{\tau_{DF}} + \frac{1}{\tau_{DF}} \frac{A_{DF} \tau_{DF}}{A_{PF} \tau_{DF}} \quad (5)$$

Lifetimes were obtained at temperatures between 300 K and 230 K in methylcyclohexane. From the slope of a plot of $\ln(k_{\text{risc}})$ versus $1/T$ (Figure 9), we obtain $\Delta E_{S-T} = 15$ meV, which is comparable to values previously reported for TADF emitters.^[143]

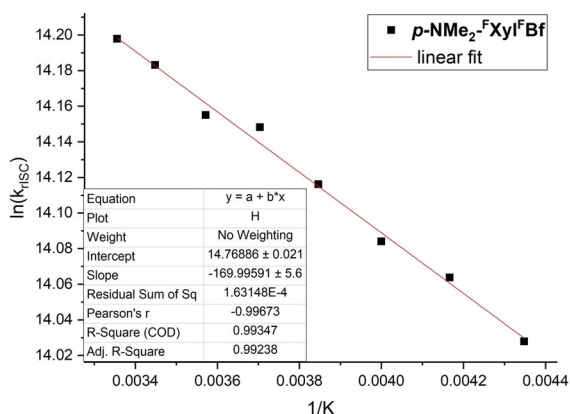


Figure 9. Arrhenius plot of $\ln(k_{\text{risc}})$ of $p\text{-NMe}_2\text{-XylBf}$ (determined from temperature-dependent lifetime measurements) vs. $1/T$.

DFT and time-dependent (TD)-DFT studies

Using the crystal structures as the starting geometries, the ground-state (GS) structures were optimized using DFT calculations at the B3LYP/6-31G+(d) level of theory. For $\text{F}^{\text{Mes}}\text{Bf}$ and $\text{F}^{\text{Xyl}}\text{Bf}$, the optimized ground-state structures exhibit C_s and C_{2v} symmetries, respectively. For $p\text{-NMe}_2\text{-XylBf}$, optimization of the GS structure with C_{2v} symmetry did not lead to a global minimum but rather to a saddle point (1 imaginary frequency remained). However, given that the C_1 structure is very close to the C_{2v} symmetry one, in both geometry and energy, and exhibits almost the same transition dipole moments, the symmetry descriptors will be used as it simplifies the discussion. The optimized structures reproduce the geometries, bond lengths, angles, and shortest B–F contacts of the crystal structures reasonably well. However, as compared to the crystal structures, the optimized structures do not exhibit bending of the *exo*-aryl out of the plane of the borafluorene backbone. Given that this torsion arises from solid-state interactions, this is to be expected. The highest occupied molecular orbital (HOMO) and lowest unoccupied molecular orbital (LUMO) energies increase from $\text{F}^{\text{Mes}}\text{Bf}$ to $\text{F}^{\text{Xyl}}\text{Bf}$ to $p\text{-NMe}_2\text{-XylBf}$ (Figure 10 and Table 5). The calculated LUMO energies fit well with the LUMO energies estimated from the reduction potentials obtained through cyclic voltammetry. Due to the very broad nature of the lowest-energy absorption band, the HOMO energies of

Table 5. Frontier molecular p-orbital energies [eV] and symmetries of $\text{F}^{\text{Mes}}\text{Bf}$, $\text{F}^{\text{Xyl}}\text{Bf}$, and $p\text{-NMe}_2\text{-XylBf}$ calculated at the B3LYP/6-31+G(d) level.

symmetry	$\text{F}^{\text{Mes}}\text{Bf}$		$\text{F}^{\text{Xyl}}\text{Bf}$		$p\text{-NMe}_2\text{-XylBf}$		
	C_s calc.	exp. ^[a]	C_{2v} calc.	exp. ^[a]	C_1 calc.	C_{2v} calc.	exp. ^[a]
LUMO+1 [eV] (sym.)	-2.66 (A'')		-2.50 (B ₁)		-2.34 (A ₁)	-2.32 (B ₁)	
LUMO [eV] (sym.)	-3.80 (A'')	-4.02	-3.60 (B ₁)	-3.95	-3.41 (A ₁)	-3.42 (B ₁)	-3.88
HOMO [eV] (sym.)	-7.65 (A'')		-7.49 (A ₂)		-6.17 (A ₁)	-6.16 (B ₂)	-6.11
HOMO-1 [eV] (sym.)	-8.49 (A')		-8.03 (B ₂)		-7.32 (A ₁)	-7.41 (A ₂)	

[a] Determined from the half-wave potentials: HOMO = $-(5.16 + E_{1/2, \text{ox}})$ eV, LUMO = $-(5.16 + E_{1/2, \text{red}})$ eV.^[122,144,145]

$\text{F}^{\text{Mes}}\text{Bf}$ and $\text{F}^{\text{Xyl}}\text{Bf}$ were not calculated from the experimental data.

The LUMOs are all localized on the borafluorene moieties with their largest components on boron, and the energies differ by only 0.2–0.4 eV. For $\text{F}^{\text{Mes}}\text{Bf}$ and $\text{F}^{\text{Xyl}}\text{Bf}$ the HOMOs are also localized on the borafluorene moieties with boron lying on a nodal plane, and are energetically similar ($\Delta E = 0.16$ eV). The HOMO of $p\text{-NMe}_2\text{-XylBf}$ is localized on the *exo*-aryl moiety and lies about 1.4 eV higher in energy than the HOMOs of $\text{F}^{\text{Mes}}\text{Bf}$ and $\text{F}^{\text{Xyl}}\text{Bf}$. This is due to the electron-donating effect of the *para*-dimethylamino-group that increases the energy of the *exo*-aryl fragment MO thereby raising it above the borafluorene-centered orbital which is now HOMO-1. For both $\text{F}^{\text{Mes}}\text{Bf}$ and $\text{F}^{\text{Xyl}}\text{Bf}$, HOMO-1 is localized on the *exo*-aryl moiety; however, due to the *para*-CF₃ group, the HOMO-1 of $\text{F}^{\text{Mes}}\text{Bf}$ is about 0.5 eV lower in energy. Based on the optimized ground-state structures the nucleus-independent chemical shift (NICS) values of the borafluorenes were calculated (Table 6).

It is apparent that the perfluoroalkylated borafluorenes exhibit lower NICS(1)_{zz} values as compared to that of the borafluorene **TipBf** which does not contain CF₃ groups. This suggests a higher degree of delocalization of the electron density over the borafluorene backbone in our compounds. Thus, the antiaromatic character is less than in non-trifluoromethylated borafluorenes. The optimized structures were then used for TD-DFT calculations to simulate the absorption spectra. Time-dependent DFT calculations on $\text{F}^{\text{Mes}}\text{Bf}$ and $\text{F}^{\text{Xyl}}\text{Bf}$ were carried out at the B3LYP/6-31+G(d) level of theory whereas for the donor substituted $p\text{-NMe}_2\text{-XylBf}$ the Coulomb-attenuated functional CAM-B3LYP was employed using the same basis set (Table 7), because CAM-B3LYP is better suited to systems involving charge transfer.^[146,147] Furthermore, the optimized S₁-state geometries of $\text{F}^{\text{Mes}}\text{Bf}$ and $\text{F}^{\text{Xyl}}\text{Bf}$ were obtained. In order to characterize the nature of the transition the overlap coefficients (λ) were determined.^[146] The calculated lowest-

Compound	NICS(1) _{zz}	
	calcd	Lit.
^F Mes ^F Bf	20.7	
^F Xyl ^F Bf	20.2	
<i>p</i> -NMe ₂ - ^F Xyl ^F Bf	20.0	
TipBf	24.3	24.5 ^[119]

energy absorptions of the borafluorenes fit well with the experimental values. For all compounds, the lowest-energy transitions are predominantly of HOMO to LUMO character.

For both ^FMes^FBf and ^FXyl^FBf these can be classified as locally excited (LE) transitions ($\lambda \approx 0.65$) as both HOMO and LUMO are localized on the borafluorene backbone. This is surprising, as LE transitions usually exhibit high extinction coefficients and

^FMes^FBf and ^FXyl^FBf exhibit weakly allowed lowest energy absorptions. However, the calculated oscillator strengths of the $S_1 \leftarrow S_0$ transitions of ^FMes^FBf and ^FXyl^FBf are also very small. From the symmetries of the frontier molecular orbitals it is possible to determine whether these transitions are forbidden by symmetry. The symmetries of the HOMOs of ^FMes^FBf (C_s) and ^FXyl^FBf (C_{2v}) are A' and A_2 , respectively, and the LUMO symmetries are A'' and B_1 . Transitions are allowed by symmetry if the initial and final states multiplied by the x -, y -, and z -characters of the electronic dipole operator contain the totally symmetric irreducible representation (C_s : A' and C_{2v} : A_1). For ^FMes^FBf (C_s), the lowest-energy transition is forbidden in the z -direction, whereas x and y are allowed, making the transition an allowed transition. For ^FXyl^FBf (C_{2v}), the x - and z -directions are forbidden, whereas the y -direction is allowed, making the transition an allowed transition. However, for both molecules, the dipole moment is oriented along the z -axis, resulting in a very small transition dipole moment in the x - and y -directions,

Table 7. Lowest-energy and highest oscillator-strength absorptions and emissions of ^FMes^FBf and ^FXyl^FBf calculated at the B3LYP/6–31+G(d) level of theory and lowest-energy absorptions of *p*-NMe₂-^FXyl^FBf calculated at the CAM-B3LYP/6–31+G(d) level of theory.

Compound	State	E [eV]	λ [nm]	λ_{exp} [nm]	f	Symmetry	Major contributions	λ
^F Mes ^F Bf (C_s)	$S_1 \leftarrow S_0$	3.05	406	400	0.0005	A'	HOMO \rightarrow LUMO (99%)	0.65
	$S_2 \leftarrow S_0$	3.90	318		0	A''	HOMO–1 \rightarrow LUMO (99%)	0.25
	$S_7 \leftarrow S_0$	4.80	258	257	0.8333	A'	HOMO–2 \rightarrow LUMO (24%), HOMO \rightarrow LUMO+1 (70%)	0.73
	$S_1 \rightarrow S_0$	2.22	559	521	0.0038	A	H-SOMO \leftarrow L-SOMO (99%)	
^F Xyl ^F Bf (C_{2v})	$S_1 \leftarrow S_0$	3.09	401	385	0.0006	B_2	HOMO \rightarrow LUMO (99%)	0.66
	$S_2 \leftarrow S_0$	3.64	340		0	A_2	HOMO–1 \rightarrow LUMO (99%)	0.23
	$S_6 \leftarrow S_0$	4.81	258	256	0.8413	B_2	HOMO–3 \rightarrow LUMO (28%), HOMO \rightarrow LUMO+1 (68%)	0.74
	$S_1 \rightarrow S_0$	2.34	531	510	0.0030	A	H-SOMO \leftarrow L-SOMO (99%)	
<i>p</i> -NMe ₂ - ^F Xyl ^F Bf (C_s)	$S_1 \leftarrow S_0$	3.25	382	396	0	A	HOMO \rightarrow LUMO (92%)	0.15
	$S_2 \leftarrow S_0$	3.46	358	326	0.0006	A	HOMO–1 \rightarrow LUMO (97%)	0.67
	$S_3 \leftarrow S_0$	4.25	292	270	0.0491	A	HOMO \rightarrow L+2 (70%), HOMO \rightarrow L+3 (24%)	0.49
	$S_8 \leftarrow S_0$	5.11	243	256	0.6022	A	HOMO \rightarrow L+4 (86%)	0.71

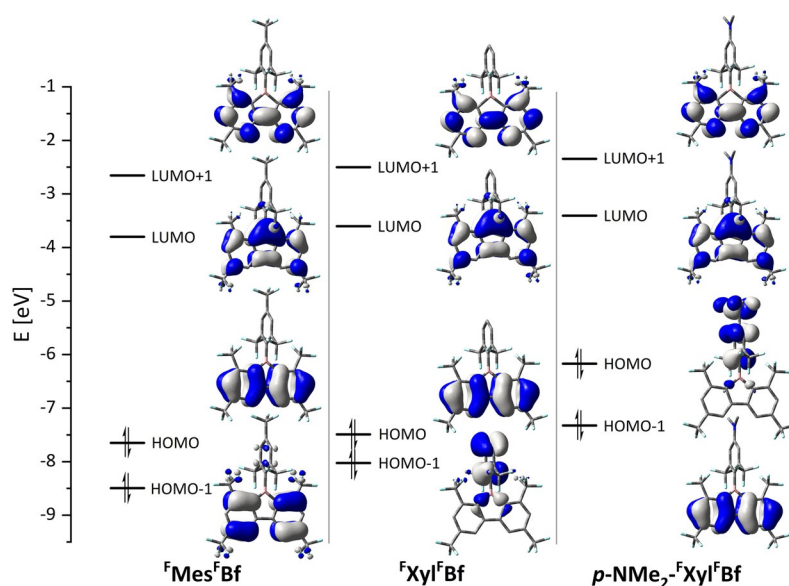


Figure 10. Frontier molecular orbitals of ^FMes^FBf (left), ^FXyl^FBf (middle), and *p*-NMe₂-^FXyl^FBf (right) calculated at the B3LYP/6–31+G(d) level of theory.

which results in very low oscillator strengths. So, the lowest-energy transitions are allowed, but exhibit only small changes in dipole moment resulting in weak absorptions. This can be, in part, attributed to the boron center, because its contribution to the LUMO gives the transition a π - n character. The $S_2 \leftarrow S_0$ transitions, in both cases, are predominantly HOMO-1 to LUMO transitions. The HOMO-1 of ${}^{\text{F}}\text{Mes}^{\text{F}}\text{Bf}$ and ${}^{\text{F}}\text{Xyl}^{\text{F}}\text{Bf}$ are of A' and B_2 symmetry, respectively, and, thus, are symmetry forbidden. Both ${}^{\text{F}}\text{Mes}^{\text{F}}\text{Bf}$ and ${}^{\text{F}}\text{Xyl}^{\text{F}}\text{Bf}$, exhibit large oscillator strengths for their $S_7 \leftarrow S_0$ and $S_6 \leftarrow S_0$ transitions, respectively. In both cases, these transitions have predominantly HOMO to LUMO+1 character. Both HOMO and LUMO+1 are delocalized over the borafluorene backbone without contributions from the boron center. The optimized S_1 geometries of ${}^{\text{F}}\text{Mes}^{\text{F}}\text{Bf}$ and ${}^{\text{F}}\text{Xyl}^{\text{F}}\text{Bf}$ differ only slightly from their ground-state structures (Figure 11).

In comparison, in the S_1 structure of ${}^{\text{F}}\text{Mes}^{\text{F}}\text{Bf}$, only the *para*- CF_3 groups on the borafluorene backbone are rotated and in both ${}^{\text{F}}\text{Mes}^{\text{F}}\text{Bf}$ and ${}^{\text{F}}\text{Xyl}^{\text{F}}\text{Bf}$ the *ortho*- CF_3 groups on the *exo*-aryl are slightly bent away from the boron center. The calculated emission maxima of ${}^{\text{F}}\text{Mes}^{\text{F}}\text{Bf}$ and ${}^{\text{F}}\text{Xyl}^{\text{F}}\text{Bf}$, fit the experimental data in hexane and also exhibit very low oscillator strengths. Even though the optimized structures do not exhibit a higher symmetry it can be assumed that a similar phenomenon as for the absorption takes place and is the reason for the observed long lifetimes. Interestingly, as previously discussed, the reasonably high quantum yields observed are due to extremely slow non-radiative decay processes.

The photophysical properties of $p\text{-NMe}_2\text{-}{}^{\text{F}}\text{Xyl}^{\text{F}}\text{Bf}$ differ strongly from those of ${}^{\text{F}}\text{Mes}^{\text{F}}\text{Bf}$ and ${}^{\text{F}}\text{Xyl}^{\text{F}}\text{Bf}$. This is, in part, due to the fact that the nature of the lowest-energy absorption has CT rather than LE character ($\lambda = 0.15$). This is not surprising, given that $p\text{-NMe}_2\text{-}{}^{\text{F}}\text{Xyl}^{\text{F}}\text{Bf}$ is a donor-acceptor system. The $S_1 \leftarrow S_0$ transition of $p\text{-NMe}_2\text{-}{}^{\text{F}}\text{Xyl}^{\text{F}}\text{Bf}$ exhibits an oscillator strength of 0. Using the optimized structure of C_{2v} symmetry as an approximation, it becomes apparent that this transition is symmetry forbidden and, furthermore, the overlap between HOMO and LUMO is minuscule due to the nearly perpendicular arrangement of the *exo*-aryl group with respect to the borafluorene core. The HOMO is of B_2 symmetry and the LUMO has B_1 symmetry. This is the same as for the $S_2 \leftarrow S_0$ transitions of

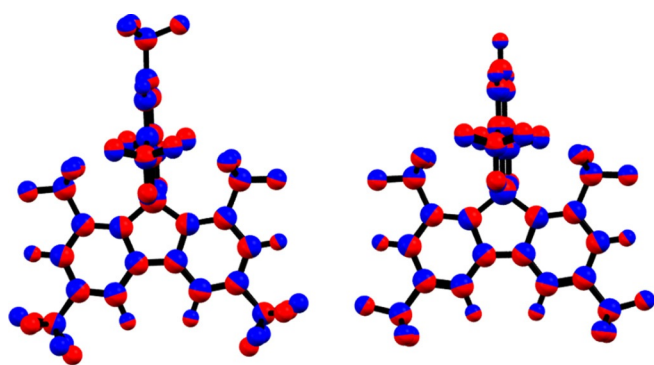


Figure 11. Overlap of the optimized ground state (blue) and S_1 (red) geometries of ${}^{\text{F}}\text{Mes}^{\text{F}}\text{Bf}$ (left) and ${}^{\text{F}}\text{Xyl}^{\text{F}}\text{Bf}$ (right).

${}^{\text{F}}\text{Mes}^{\text{F}}\text{Bf}$ and ${}^{\text{F}}\text{Xyl}^{\text{F}}\text{Bf}$, because the HOMO and HOMO-1 are inverted compared to those of $p\text{-NMe}_2\text{-}{}^{\text{F}}\text{Xyl}^{\text{F}}\text{Bf}$. For $p\text{-NMe}_2\text{-}{}^{\text{F}}\text{Xyl}^{\text{F}}\text{Bf}$, however, the $S_2 \leftarrow S_0$ transition is allowed, but analogously to the ${}^{\text{F}}\text{Mes}^{\text{F}}\text{Bf}$ and ${}^{\text{F}}\text{Xyl}^{\text{F}}\text{Bf}$ cases, exhibits a very low oscillator strength. This explains the low extinction coefficient observed for the lowest-energy absorption of $p\text{-NMe}_2\text{-}{}^{\text{F}}\text{Xyl}^{\text{F}}\text{Bf}$. Furthermore, we optimized the S_1 structure of $p\text{-NMe}_2\text{-}{}^{\text{F}}\text{Xyl}^{\text{F}}\text{Bf}$ as well as its T_1 structure in order to calculate the $S_1\text{-}T_1$ energy gap. Both optimizations were carried out using the PCM solvent-correction model due to the charge-transfer nature of the transitions and the high dipole moment of both S_1 and T_1 . Comparing the energies of both structures results in $\Delta E_{S_1-T_1} = 423$ meV which is almost 30 times higher than the experimentally determined gap. It is noteworthy that the experimental determination of the gap is highly flawed due to approximations as well as unpredictable solvent effects at lower temperature. However, this should still give a good estimate, but the calculations fail to match the experimental value at this level of theory, illustrating the difficulty of predicting phenomena such as TADF accurately.

Conclusions

Herein, we reported the synthesis and properties of three trifluoromethylated borafluorenes ${}^{\text{F}}\text{Mes}^{\text{F}}\text{Bf}$, ${}^{\text{F}}\text{Xyl}^{\text{F}}\text{Bf}$, and $p\text{-NMe}_2\text{-}{}^{\text{F}}\text{Xyl}^{\text{F}}\text{Bf}$. The copper-catalyzed homocoupling of boronate esters provides a convenient route to 2,2'-dibromobiphenyl derivatives, which can be lithiated and then reacted with stable and accessible aryl- BF_3K salts for the synthesis of borafluorenes. All of the borafluorenes exhibit a rigid geometry with the *exo*-aryl group lying perpendicular to the borafluorene plane. All three borafluorenes exhibit exceptionally positively shifted reduction potentials, emphasizing the electron-withdrawing nature of the CF_3 groups. This allowed us to use a mild reducing agent (CoCp_2 $E^0 = -1.3$ eV vs. Fc/Fc^+) to reduce the most anodically shifted borafluorene ${}^{\text{F}}\text{Mes}^{\text{F}}\text{Bf}$. The resulting radical anion of ${}^{\text{F}}\text{Mes}^{\text{F}}\text{Bf}$ exhibits a strong delocalization of the additional electron over the borafluorene backbone as evidenced by EPR spectroscopy and its solid-state structure. The trifluoromethylated borafluorenes exhibit unusually long excited-state lifetimes and weakly allowed lowest-energy transitions. For ${}^{\text{F}}\text{Mes}^{\text{F}}\text{Bf}$ and ${}^{\text{F}}\text{Xyl}^{\text{F}}\text{Bf}$, this is the result of the transitions being forbidden in the z -direction which coincides with the dipole moment and the transition dipole moment being negligible in the x - and y -directions. The same is apparently true for their emissions, as both compounds exhibit fluorescence lifetimes of $\tau > 200$ ns in hexane. Even with small oscillator strengths, the two compounds exhibit fluorescence quantum yields of 0.37 and 0.30, respectively, because their rigidity results in exceptionally slow non-radiative decay. In contrast, the twisted donor-acceptor system $p\text{-NMe}_2\text{-}{}^{\text{F}}\text{Xyl}^{\text{F}}\text{Bf}$ has a symmetry forbidden lowest-energy transition and exhibits TADF, with a singlet-triplet energy gap $\Delta E_{S_1-T_1}$ experimentally determined to be only 15 meV. The compounds ${}^{\text{F}}\text{Mes}^{\text{F}}\text{Bf}$ and ${}^{\text{F}}\text{Xyl}^{\text{F}}\text{Bf}$ are highly stable towards hydrolysis, which makes them interesting potential building blocks for organic materials.

Acknowledgements

We thank the Julius-Maximilians-Universität of Würzburg, the Deutsche Forschungsgemeinschaft (MA4471/8-1) and the Bavarian State Ministry of Science, Research, and the Arts for the Collaborative Research Network “Solar Technologies go Hybrid” for financial support, and the Bavarian Academy of Science and Humanities for access to the Linux-Cluster of the Leibniz Supercomputing Centre. We are grateful for a generous donation of B₂pin₂ from AllyChem. Co. Ltd. The authors thank Christoph Mahler and Robert Ricker for HRMS measurements, Dr. Rüdiger Bertermann for NMR measurements, and Dr. Jörn Nitsch and Dr. Julia Merz for helpful discussions. Open access funding enabled and organized by Projekt DEAL.

Conflict of interest

The authors declare no conflict of interest.

Keywords: boraflorenes • boron • EPR spectroscopy • fluorescence • heterocycles

- [1] C. D. Entwistle, T. B. Marder, *Angew. Chem. Int. Ed.* **2002**, *41*, 2927–2931; *Angew. Chem.* **2002**, *114*, 3051–3056.
- [2] C. D. Entwistle, T. B. Marder, *Chem. Mater.* **2004**, *16*, 4574–4585.
- [3] S. Yamaguchi, A. Wakamiya, *Pure Appl. Chem.* **2006**, *78*, 1413.
- [4] F. Jäkle, *Coord. Chem. Rev.* **2006**, *250*, 1107–1121.
- [5] R. Stahl, C. Lambert, C. Kaiser, R. Wortmann, R. Jakober, *Chem. Eur. J.* **2006**, *12*, 2358–2370.
- [6] M. Elbing, G. C. Bazan, *Angew. Chem. Int. Ed.* **2008**, *47*, 834–838; *Angew. Chem.* **2008**, *120*, 846–850.
- [7] Z. M. Hudson, S. Wang, *Acc. Chem. Res.* **2009**, *42*, 1584–1596.
- [8] C. R. Wade, A. E. J. Broomsgrove, S. Aldridge, F. P. Gabbaï, *Chem. Rev.* **2010**, *110*, 3958–3984.
- [9] Z. M. Hudson, S. Wang, *Dalton Trans.* **2011**, *40*, 7805–7816.
- [10] A. Wakamiya, S. Yamaguchi, *Bull. Chem. Soc. Jpn.* **2015**, *88*, 1357–1377.
- [11] L. Ji, S. Griesbeck, T. B. Marder, *Chem. Sci.* **2017**, *8*, 846–863.
- [12] S.-Y. Li, Z.-B. Sun, C.-H. Zhao, *Inorg. Chem.* **2017**, *56*, 8705–8717.
- [13] G. Turkoglu, M. E. Cinar, T. Ozturk, *Molecules* **2017**, *22*, 1522.
- [14] C. Dou, S. Saito, K. Matsuo, I. Hisaki, S. Yamaguchi, *Angew. Chem. Int. Ed.* **2012**, *51*, 12206–12210; *Angew. Chem.* **2012**, *124*, 12372–12376.
- [15] C. Hoffend, M. Diefenbach, E. Januszewski, M. Bolte, H. W. Lerner, M. C. Holthausen, M. Wagner, *Dalton Trans.* **2013**, *42*, 13826–13837.
- [16] A. Escande, M. J. Ingleson, *Chem. Commun.* **2015**, *51*, 6257–6274.
- [17] V. M. Hertz, N. Ando, M. Hirai, M. Bolte, H.-W. Lerner, S. Yamaguchi, M. Wagner, *Organometallics* **2016**, *35*, 2512–2519.
- [18] B. Su, R. Kinjo, *Synthesis* **2017**, *49*, 2985–3034.
- [19] E. von Grotthuss, A. John, T. Kaese, M. Wagner, *Asian J. Org. Chem.* **2018**, *7*, 37–53.
- [20] Y. Su, R. Kinjo, *Chem. Soc. Rev.* **2019**, *48*, 3613–3659.
- [21] N. Matsumi, K. Naka, Y. Chujo, *J. Am. Chem. Soc.* **1998**, *120*, 5112–5113.
- [22] S. Yamaguchi, S. Akiyama, K. Tamao, *J. Am. Chem. Soc.* **2000**, *122*, 6335–6336.
- [23] W.-L. Jia, D. Song, S. Wang, *J. Org. Chem.* **2003**, *68*, 701–705.
- [24] A. Wakamiya, T. Ide, S. Yamaguchi, *J. Am. Chem. Soc.* **2005**, *127*, 14859–14866.
- [25] I. Yamaguchi, B.-J. Choi, T.-A. Koizumi, K. Kubota, T. Yamamoto, *Macromolecules* **2007**, *40*, 438–443.
- [26] U. Megerle, F. Selmaier, C. Lambert, E. Riedle, S. Lochbrunner, *Phys. Chem. Chem. Phys.* **2008**, *10*, 6245–6251.
- [27] A. Lorbach, M. Bolte, H. Li, H.-W. Lerner, M. C. Holthausen, F. Jäkle, M. Wagner, *Angew. Chem. Int. Ed.* **2009**, *48*, 4584–4588; *Angew. Chem.* **2009**, *121*, 4654–4658.
- [28] L. Weber, V. Werner, M. A. Fox, T. B. Marder, S. Schwedler, A. Brockhinke, H.-G. Stammler, B. Neumann, *Dalton Trans.* **2009**, 2823–2831.
- [29] L. Weber, D. Eickhoff, T. B. Marder, M. A. Fox, P. J. Low, A. D. Dwyer, D. J. Tozer, S. Schwedler, A. Brockhinke, H.-G. Stammler, B. Neumann, *Chem. Eur. J.* **2012**, *18*, 1369–1382.
- [30] Z. Zhou, A. Wakamiya, T. Kushida, S. Yamaguchi, *J. Am. Chem. Soc.* **2012**, *134*, 4529–4532.
- [31] C. Reus, S. Weidlich, M. Bolte, H.-W. Lerner, M. Wagner, *J. Am. Chem. Soc.* **2013**, *135*, 12892–12907.
- [32] J. Yoshino, Y. Nakamura, S. Kunitomo, N. Hayashi, H. Higuchi, *Tetrahedron Lett.* **2013**, *54*, 2817–2820.
- [33] X. Yin, J. Chen, R. A. Lalancette, T. B. Marder, F. Jäkle, *Angew. Chem. Int. Ed.* **2014**, *53*, 9761–9765; *Angew. Chem.* **2014**, *126*, 9919–9923.
- [34] A. Ito, K. Kawanishi, E. Sakuda, N. Kitamura, *Chem. Eur. J.* **2014**, *20*, 3940–3953.
- [35] Z. Zhang, R. M. Edkins, J. Nitsch, K. Fucke, A. Eichhorn, A. Steffen, Y. Wang, T. B. Marder, *Chem. Eur. J.* **2015**, *21*, 177–190.
- [36] J. Merz, J. Fink, A. Friedrich, I. Krummenacher, H. H. Al Mamari, S. Lorenzen, M. Haehnel, A. Eichhorn, M. Moos, M. Holzapfel, H. Braunschweig, C. Lambert, A. Steffen, L. Ji, T. B. Marder, *Chem. Eur. J.* **2017**, *23*, 13164–13180.
- [37] S. Griesbeck, E. Michail, C. Wang, H. Ogasawara, S. Lorenzen, L. Gerstner, T. Zang, J. Nitsch, Y. Sato, R. Bertermann, M. Taki, C. Lambert, S. Yamaguchi, T. B. Marder, *Chem. Sci.* **2019**, *10*, 5405–5422.
- [38] X. Jia, J. Nitsch, L. Ji, Z. Wu, A. Friedrich, F. Kerner, M. Moos, C. Lambert, T. B. Marder, *Chem. Eur. J.* **2019**, *25*, 10845–10857.
- [39] J. Merz, A. Steffen, J. Nitsch, J. Fink, C. B. Schürger, A. Friedrich, I. Krummenacher, H. Braunschweig, M. Moos, D. Mims, C. Lambert, T. B. Marder, *Chem. Sci.* **2019**, *10*, 7516–7534.
- [40] J. He, F. Rauch, A. Friedrich, D. Sieh, T. Ribbeck, I. Krummenacher, H. Braunschweig, M. Finze, T. B. Marder, *Chem. Eur. J.* **2019**, *25*, 13777–13784.
- [41] Z. Yuan, N. J. Taylor, T. B. Marder, I. D. Williams, S. K. Kurtz, L.-T. Cheng, *J. Chem. Soc. Chem. Commun.* **1990**, 1489–1492.
- [42] Z. Yuan, N. J. Taylor, Y. Sun, T. B. Marder, I. D. Williams, L.-T. Cheng, *J. Organomet. Chem.* **1993**, *449*, 27–37.
- [43] Z. Yuan, N. J. Taylor, R. Ramachandran, T. B. Marder, *Appl. Organomet. Chem.* **1996**, *10*, 305–316.
- [44] Z.-Q. Liu, Q. Fang, D. Wang, G. Xue, W.-T. Yu, Z.-S. Shao, M.-H. Jiang, *Chem. Commun.* **2002**, 2900–2901.
- [45] Z.-Q. Liu, Q. Fang, D. Wang, D.-X. Cao, G. Xue, W.-T. Yu, H. Lei, *Chem. Eur. J.* **2003**, *9*, 5074–5084.
- [46] M. Charlot, L. Porres, C. D. Entwistle, A. Beeby, T. B. Marder, M. Blanchard-Desce, *Phys. Chem. Chem. Phys.* **2005**, *7*, 600–606.
- [47] Z. Yuan, C. D. Entwistle, J. C. Collings, D. Albesa-Jové, A. S. Batsanov, J. A. K. Howard, N. J. Taylor, H. M. Kaiser, D. E. Kaufmann, S.-Y. Poon, W.-Y. Wong, C. Jardin, S. Fathallah, A. Boucekkine, J.-F. Halet, T. B. Marder, *Chem. Eur. J.* **2006**, *12*, 2758–2771.
- [48] C. D. Entwistle, J. C. Collings, A. Steffen, L.-O. Pålsson, A. Beeby, D. Albesa-Jové, J. M. Burke, A. S. Batsanov, J. A. K. Howard, J. A. Mosely, S.-Y. Poon, W.-Y. Wong, F. Ibersiene, S. Fathallah, A. Boucekkine, J.-F. Halet, T. B. Marder, *J. Mater. Chem.* **2009**, *19*, 7532–7544.
- [49] J. C. Collings, S.-Y. Poon, C. Le Droumaguet, M. Charlot, C. Katan, L.-O. Pålsson, A. Beeby, J. A. Mosely, H. M. Kaiser, D. Kaufmann, W.-Y. Wong, M. Blanchard-Desce, T. B. Marder, *Chem. Eur. J.* **2009**, *15*, 198–208.
- [50] L. Ji, R. M. Edkins, L. J. Sewell, A. Beeby, A. S. Batsanov, K. Fucke, M. Drafz, J. A. K. Howard, O. Moutounet, F. Ibersiene, A. Boucekkine, E. Furet, Z. Liu, J.-F. Halet, C. Katan, T. B. Marder, *Chem. Eur. J.* **2014**, *20*, 13618–13635.
- [51] P. Chen, A. S. Marshall, S. H. Chi, X. Yin, J. W. Perry, F. Jakle, *Chem. Eur. J.* **2015**, *21*, 18237–18247.
- [52] S. Griesbeck, Z. Zhang, M. Gutmann, T. Lühmann, R. M. Edkins, G. Clermont, A. N. Lazar, M. Haehnel, K. Edkins, A. Eichhorn, M. Blanchard-Desce, L. Meinel, T. B. Marder, *Chem. Eur. J.* **2016**, *22*, 14701–14706.
- [53] S. Griesbeck, E. Michail, F. Rauch, H. Ogasawara, C. Wang, Y. Sato, R. M. Edkins, Z. Zhang, M. Taki, C. Lambert, S. Yamaguchi, T. B. Marder, *Chem. Eur. J.* **2019**, *25*, 13164–13175.
- [54] S. Yamaguchi, S. Akiyama, K. Tamao, *J. Am. Chem. Soc.* **2001**, *123*, 11372–11375.
- [55] T. W. Hudnall, C.-W. Chiu, F. P. Gabbaï, *Acc. Chem. Res.* **2009**, *42*, 388–397.

- [56] K. Parab, K. Venkatasubbaiah, F. Jäkle, *J. Am. Chem. Soc.* **2006**, *128*, 12879–12885.
- [57] G. C. Welch, R. R. S. Juan, J. D. Masuda, D. W. Stephan, *Science* **2006**, *314*, 1124–1126.
- [58] G. C. Welch, D. W. Stephan, *J. Am. Chem. Soc.* **2007**, *129*, 1880–1881.
- [59] S. J. Geier, D. W. Stephan, *J. Am. Chem. Soc.* **2009**, *131*, 3476–3477.
- [60] D. W. Stephan, G. Erker, *Angew. Chem. Int. Ed.* **2010**, *49*, 46–76; *Angew. Chem.* **2010**, *122*, 50–81.
- [61] D. W. Stephan, G. Erker, *Chem. Sci.* **2014**, *5*, 2625–2641.
- [62] D. W. Stephan, *J. Am. Chem. Soc.* **2015**, *137*, 10018–10032.
- [63] D. W. Stephan, G. Erker, *Angew. Chem. Int. Ed.* **2015**, *54*, 6400–6441; *Angew. Chem.* **2015**, *127*, 6498–6541.
- [64] Y. Shirota, *J. Mater. Chem.* **2000**, *10*, 1–25.
- [65] A. Wakamiya, K. Mori, S. Yamaguchi, *Angew. Chem. Int. Ed.* **2007**, *46*, 4273–4276; *Angew. Chem.* **2007**, *119*, 4351–4354.
- [66] K. Suzuki, S. Kubo, K. Shizu, T. Fukushima, A. Wakamiya, Y. Murata, C. Adachi, H. Kaji, *Angew. Chem. Int. Ed.* **2015**, *54*, 15231–15235; *Angew. Chem.* **2015**, *127*, 15446–15450.
- [67] J. J. Eisch, N. K. Hota, S. Kozima, *J. Am. Chem. Soc.* **1969**, *91*, 4575–4577.
- [68] J. J. Eisch, J. E. Galle, S. Kozima, *J. Am. Chem. Soc.* **1986**, *108*, 379–385.
- [69] S. Kim, K.-H. Song, S. O. Kang, J. Ko, *Chem. Commun.* **2004**, 68–69.
- [70] H. Braunschweig, I. Fernández, G. Frenking, T. Kupfer, *Angew. Chem. Int. Ed.* **2008**, *47*, 1951–1954; *Angew. Chem.* **2008**, *120*, 1977–1980.
- [71] C. Fan, W. E. Piers, M. Parvez, *Angew. Chem. Int. Ed.* **2009**, *48*, 2955–2958; *Angew. Chem.* **2009**, *121*, 2999–3002.
- [72] J. Köhler, S. Lindenmeier, I. Fischer, H. Braunschweig, T. Kupfer, D. Gamon, C.-W. Chiu, *J. Raman Spectrosc.* **2010**, *41*, 636–641.
- [73] A. Steffen, R. M. Ward, W. D. Jones, T. B. Marder, *Coord. Chem. Rev.* **2010**, *254*, 1950–1976.
- [74] H. Braunschweig, T. Kupfer, *Chem. Commun.* **2011**, *47*, 10903–10914.
- [75] H. Braunschweig, C.-W. Chiu, D. Gamon, M. Kaupp, I. Krummenacher, T. Kupfer, R. Müller, K. Radacki, *Chem. Eur. J.* **2012**, *18*, 11732–11746.
- [76] T. Araki, A. Fukazawa, S. Yamaguchi, *Angew. Chem. Int. Ed.* **2012**, *51*, 5484–5487; *Angew. Chem.* **2012**, *124*, 5580–5583.
- [77] H. Braunschweig, I. Krummenacher, J. Wahler, *Adv. Organomet. Chem.* **2013**, *61*, 1–53.
- [78] H. Braunschweig, C. Hörl, L. Mailänder, K. Radacki, J. Wahler, *Chem. Eur. J.* **2014**, *20*, 9858–9861.
- [79] Z. Zhang, R. M. Edkins, M. Haehnel, M. Wehner, A. Eichhorn, L. Mailänder, M. Meier, J. Brand, F. Brede, K. Müller-Buschbaum, H. Braunschweig, T. B. Marder, *Chem. Sci.* **2015**, *6*, 5922–5927.
- [80] J. H. Barnard, S. Yruegas, K. Huang, C. D. Martin, *Chem. Commun.* **2016**, *52*, 9985–9991.
- [81] W. Zhang, B. Zhang, D. Yu, G. He, *Sci. Bull.* **2017**, *62*, 899–900.
- [82] M. Meier, L. Ji, J. Nitsch, I. Krummenacher, A. Deißberger, D. Auerhammer, M. Schäfer, T. B. Marder, H. Braunschweig, *Chem. Eur. J.* **2019**, *25*, 4707–4712.
- [83] H. C. Brown, V. H. Dodson, *J. Am. Chem. Soc.* **1957**, *79*, 2302–2306.
- [84] P. J. Grisdale, J. L. R. Williams, M. E. Glogowski, B. E. Babb, *J. Org. Chem.* **1971**, *36*, 544–549.
- [85] H. Braunschweig, V. Dyakonov, J. O. C. Jimenez-Halla, K. Kraft, I. Krummenacher, K. Radacki, A. Sperlich, J. Wahler, *Angew. Chem. Int. Ed.* **2012**, *51*, 2977–2980; *Angew. Chem.* **2012**, *124*, 3031–3034.
- [86] S. Yamaguchi, T. Shirasaka, S. Akiyama, K. Tamao, *J. Am. Chem. Soc.* **2002**, *124*, 8816–8817.
- [87] A. Wakamiya, K. Mishima, K. Ekawa, S. Yamaguchi, *Chem. Commun.* **2008**, 579–581.
- [88] M. F. Smith, S. J. Cassidy, I. A. Adams, M. Vasiliu, D. L. Gerlach, D. A. Dixon, P. A. Rugar, *Organometallics* **2016**, *35*, 3182–3191.
- [89] S. J. Cassidy, I. Brettell-Adams, L. E. McNamara, M. F. Smith, M. Bautista, H. Cao, M. Vasiliu, D. L. Gerlach, F. Qu, N. I. Hammer, D. A. Dixon, P. A. Rugar, *Organometallics* **2018**, *37*, 3732–3741.
- [90] S. Yruegas, J. J. Martinez, C. D. Martin, *Chem. Commun.* **2018**, *54*, 6808–6811.
- [91] K. R. Bluer, L. E. Laperriere, A. Pujol, S. Yruegas, V. A. K. Adiraju, C. D. Martin, *Organometallics* **2018**, *37*, 2917–2927.
- [92] S. Yruegas, J. H. Barnard, K. Al-Furaiji, J. L. Dutton, D. J. D. Wilson, C. D. Martin, *Organometallics* **2018**, *37*, 1515–1518.
- [93] T. A. Bartholome, K. R. Bluer, C. D. Martin, *Dalton Trans.* **2019**, *48*, 6319–6322.
- [94] L. E. Laperriere, S. Yruegas, C. D. Martin, *Tetrahedron* **2019**, *75*, 937–943.
- [95] P. A. Chase, P. E. Romero, W. E. Piers, M. Parvez, B. O. Patrick, *Can. J. Chem.* **2005**, *83*, 2098–2105.
- [96] P. A. Chase, W. E. Piers, B. O. Patrick, *J. Am. Chem. Soc.* **2000**, *122*, 12911–12912.
- [97] I. A. Adams, P. A. Rugar, *Macromol. Rapid Commun.* **2015**, *36*, 1336–1340.
- [98] T. Shinji, A. Mitsuhiro, O. Michinori, T. Fumio, *Bull. Chem. Soc. Jpn.* **2000**, *73*, 2357–2362.
- [99] J. Wang, Y. Wang, T. Taniguchi, S. Yamaguchi, S. Irle, *J. Phys. Chem. A* **2012**, *116*, 1151–1158.
- [100] Z. Zhang, R. M. Edkins, J. Nitsch, K. Fucke, A. Steffen, L. E. Longobardi, D. W. Stephan, C. Lambert, T. B. Marder, *Chem. Sci.* **2015**, *6*, 308–321.
- [101] X. Yin, F. Guo, R. A. Lalancette, F. Jäkle, *Macromolecules* **2016**, *49*, 537–546.
- [102] R. J. Blagg, E. J. Lawrence, K. Resner, V. S. Oganessian, T. J. Herrington, A. E. Ashley, G. G. Wildgoose, *Dalton Trans.* **2016**, *45*, 6023–6031.
- [103] M. Mantina, A. C. Chamberlin, R. Valero, C. J. Cramer, D. G. Truhlar, *J. Phys. Chem. A* **2009**, *113*, 5806–5812.
- [104] C. J. Berger, G. He, C. Merten, R. McDonald, M. J. Ferguson, E. Rivard, *Inorg. Chem.* **2014**, *53*, 1475–1486.
- [105] W. Yang, K. E. Krantz, L. A. Freeman, D. A. Dickie, A. Molino, A. Kaur, D. J. D. Wilson, R. J. Gilliard, Jr., *Chem. Eur. J.* **2019**, *25*, 12512–12516.
- [106] T. Ishiyama, J. Takagi, K. Ishida, N. Miyaura, N. R. Anastasi, J. F. Hartwig, *J. Am. Chem. Soc.* **2002**, *124*, 390–391.
- [107] I. A. I. Mkhaliid, J. H. Barnard, T. B. Marder, J. M. Murphy, J. F. Hartwig, *Chem. Rev.* **2010**, *110*, 890–931.
- [108] K. Schickedanz, T. Trageser, M. Bolte, H.-W. Lerner, M. Wagner, *Chem. Commun.* **2015**, *51*, 15808–15810.
- [109] K. Schickedanz, J. Radtke, M. Bolte, H.-W. Lerner, M. Wagner, *J. Am. Chem. Soc.* **2017**, *139*, 2842–2851.
- [110] S. Konishi, T. Iwai, M. Sawamura, *Organometallics* **2018**, *37*, 1876–1883.
- [111] M. W. Drover, K. Nagata, J. C. Peters, *Chem. Commun.* **2018**, *54*, 7916–7919.
- [112] G. A. Molander, *J. Org. Chem.* **2015**, *80*, 7837–7848.
- [113] A. J. J. Lennox, G. C. Lloyd-Jones, *Chem. Soc. Rev.* **2014**, *43*, 412–443.
- [114] S. M. Cornet, K. B. Dillon, C. D. Entwistle, M. A. Fox, A. E. Goeta, H. P. Goodwin, T. B. Marder, A. L. Thompson, *Dalton Trans.* **2003**, 4395–4405.
- [115] R. J. Blagg, T. R. Simmons, G. R. Hatton, J. M. Courtney, E. L. Bennett, E. J. Lawrence, G. G. Wildgoose, *Dalton Trans.* **2016**, *45*, 6032–6043.
- [116] H. Jacobsen, H. Berke, S. Döring, G. Kehr, G. Erker, R. Fröhlich, O. Meyer, *Organometallics* **1999**, *18*, 1724–1735.
- [117] H. Braunschweig, I. Krummenacher, *Electrochemical Behavior and Redox Chemistry of Boroles*, in *Organic Redox Systems* (Ed.: T. Nishinaga), Wiley, New York, **2015**, pp. 503–522.
- [118] P. Bissinger, H. Braunschweig, A. Damme, C. Hörl, I. Krummenacher, T. Kupfer, *Angew. Chem. Int. Ed.* **2015**, *54*, 359–362; *Angew. Chem.* **2015**, *127*, 366–369.
- [119] A. Iida, S. Yamaguchi, *J. Am. Chem. Soc.* **2011**, *133*, 6952–6955.
- [120] J. M. Farrell, C. Mützel, D. Bialas, M. Rudolf, K. Menekse, A.-M. Krause, M. Stolte, F. Würthner, *J. Am. Chem. Soc.* **2019**, *141*, 9096–9104.
- [121] S. A. Cummings, M. Iimura, C. J. Harlan, R. J. Kwaan, I. V. Trieu, J. R. Norton, B. M. Bridgewater, F. Jäkle, A. Sundararaman, M. Tilset, *Organometallics* **2006**, *25*, 1565–1568.
- [122] N. G. Connelly, W. E. Geiger, *Chem. Rev.* **1996**, *96*, 877–910.
- [123] H. Braunschweig, F. Breher, C.-W. Chiu, D. Gamon, D. Nied, K. Radacki, *Angew. Chem. Int. Ed.* **2010**, *49*, 8975–8978; *Angew. Chem.* **2010**, *122*, 9159–9162.
- [124] K. M. M. Josef, *Lichtabsorption und Photochemie organischer Moleküle*, VCH, Weinheim, **1989**.
- [125] A. G. Crawford, A. D. Dwyer, Z. Liu, A. Steffen, A. Beeby, L.-O. Pålsson, D. J. Tozer, T. B. Marder, *J. Am. Chem. Soc.* **2011**, *133*, 13349–13362.
- [126] T. M. Figueira-Duarte, K. Müllen, *Chem. Rev.* **2011**, *111*, 7260–7314.
- [127] M. K. Manna, S. Shokri, G. P. Wiederrecht, D. J. Gosztola, A. J.-L. Ayitou, *Chem. Commun.* **2018**, *54*, 5809–5818.
- [128] C.-C. Tsai, W.-C. Huang, H.-Y. Chih, Y.-C. Hsh, C.-W. Liao, C.-H. Lin, Y.-X. Kang, C.-H. Chang, Y. J. Chang, C.-W. Lu, *Org. Electron.* **2018**, *63*, 166–174.

- [129] T. Hatakeyama, K. Shiren, K. Nakajima, S. Nomura, S. Nakatsuka, K. Kinoshita, J. Ni, Y. Ono, T. Ikuta, *Adv. Mater.* **2016**, *28*, 2777–2781.
- [130] M.-Y. Zhang, Z.-Y. Li, B. Lu, Y. Wang, Y.-D. Ma, C.-H. Zhao, *Org. Lett.* **2018**, *20*, 6868–6871.
- [131] T.-L. Wu, M.-J. Huang, C.-C. Lin, P.-Y. Huang, T.-Y. Chou, R.-W. Chen-Cheng, H.-W. Lin, R.-S. Liu, C.-H. Cheng, *Nat. Photonics* **2018**, *12*, 235–240.
- [132] I. S. Park, K. Matsuo, N. Aizawa, T. Yasuda, *Adv. Funct. Mater.* **2018**, *28*, 1802031.
- [133] S.-Y. Li, Z.-B. Sun, C.-H. Zhao, *ACS Omega* **2018**, *3*, 12730–12736.
- [134] D.-G. Chen, T.-C. Lin, C.-L. Chen, Y.-T. Chen, Y.-A. Chen, G.-H. Lee, P.-T. Chou, C.-W. Liao, P.-C. Chiu, C.-H. Chang, Y.-J. Lien, Y. Chi, *ACS Appl. Mater. Interfaces* **2018**, *10*, 12886–12896.
- [135] C. Tu, W. Liang, *ACS Omega* **2017**, *2*, 3098–3109.
- [136] Y.-J. Lien, T.-C. Lin, C.-C. Yang, Y.-C. Chiang, C.-H. Chang, S.-H. Liu, Y.-T. Chen, G.-H. Lee, P.-T. Chou, C.-W. Lu, Y. Chi, *ACS Appl. Mater. Interfaces* **2017**, *9*, 27090–27101.
- [137] Y. H. Lee, S. Park, J. Oh, J. W. Shin, J. Jung, S. Yoo, M. H. Lee, *ACS Appl. Mater. Interfaces* **2017**, *9*, 24035–24042.
- [138] Y. Kitamoto, T. Namikawa, T. Suzuki, Y. Miyata, H. Kita, T. Sato, S. Oi, *Org. Electron.* **2016**, *34*, 208–217.
- [139] M. Numata, T. Yasuda, C. Adachi, *Chem. Commun.* **2015**, *51*, 9443–9446.
- [140] Y. Kitamoto, T. Namikawa, D. Ikemizu, Y. Miyata, T. Suzuki, H. Kita, T. Sato, S. Oi, *J. Mater. Chem. C* **2015**, *3*, 9122–9130.
- [141] M. Stanoppi, A. Lorbach, *Dalton Trans.* **2018**, *47*, 10394–10398.
- [142] Y. Liu, C. Li, Z. Ren, S. Yan, M. R. Bryce, *Nat. Rev. Mater.* **2018**, *3*, 18020.
- [143] F. B. Dias, T. J. Penfold, A. P. Monkman, *Methods Appl. Fluores.* **2017**, *5*, 012001.
- [144] D. Reitzenstein, T. Quast, F. Kanal, M. Kullmann, S. Ruetzel, M. S. Hammer, C. Deibel, V. Dyakonov, T. Brixner, C. Lambert, *Chem. Mater.* **2010**, *22*, 6641–6655.
- [145] D. Tsiplakides, D. Archonta, C. G. Vayenas, *Top. Catal.* **2007**, *44*, 469–479.
- [146] M. J. G. Peach, P. Benfield, T. Helgaker, D. J. Tozer, *J. Chem. Phys.* **2008**, *128*, 044118.
- [147] T. Yanai, D. P. Tew, N. C. Handy, *Chem. Phys. Lett.* **2004**, *393*, 51–57.

Manuscript received: December 9, 2019

Accepted manuscript online: January 30, 2020

Version of record online: September 21, 2020